2003

Stress intensity factors for cracks in anisotropic materials using enriched finite elements

Umit Ozkan
Lehigh University

Ozkan, Umit

Stress Intensity Factors for Cracks in Anisotropic Materials Using Enriched Finite Elements

May 2003

Stress Intensity Factors for Cracks in Anisotropic Materials Using Enriched Finite Elements

by

Umit Ozkan

A Thesis

Presented to the Graduate and Research Committee

of Lehigh University

in Candidacy for the Degree of

Master of Science

in

Mechanical Engineering

Lehigh University

(May 2003)

This thesis is accepted and approved in partial fulfillment of the requirements for the Master of Science

April 25, 2003
Date

Thesis Advisor

Chairperson of Department

Acknowledgments

This study was made possible by the financial support from the Semiconductor Research Corporation (SRC) and GE's Corporate Research and Development Center

The author wishes to express his grateful appreciation and thanks to his advisor, Prof. Herman F. Nied, for his continuous support and valuable guidance throughout the M.S. study.

The author also wishes to thank to his family for their continuous encouragement and support. Thanks are also due to my friends for their every kind of contributions and support.

Table of Contents

List of Tables

List of Figures

Abstract

Since many technologically important materials exhibit a high degree of anisotropy, it is very important that anisotropic stress intensity factors be computed correctly for these materials. Most of these materials are inherently three dimensional in nature. An enriched finite element approach is shown to be a very effective technique for obtaining stress intensity factors for these three-dimensional crack problems. This formulation utilizes the correct asymptotic crack tip stress field, for direct computation of the pertinent fracture parameters, i.e., stress intensity factors and strain energy release rates. Of particular importance in the anisotropic case, is inclusion of asymptotic generalized plane deformation behavior. The generalized plane deformation formulation demonstrates that even when the loading is normal to the crack surface, the resulting stress state can be fully three-dimensional, i.e., all fracture modes are present. This effect is due solely to the material anisotropy and is not observed in isotropic crack problems. Example solutions for three-dimensional crack problems in anisotropic materials are compared with those of identical three-dimensional cracks in isotropic materials. The difference between these two cases and the consequences for reliability predictions in engineering design is discussed.

Chapter 1

Introduction

With the advent of modern technology, the material sciences have become increasingly concerned with the importance of anisotropic materials and with the failures of anisotropic materials due to fracture [2]. Most of the materials used in electronic packages contain some degree of anisotropy. Also single crystal materials used in advanced engineering materials are highly anisotropic. In addition, composite materials, which are used very extensively in advance structures, have a high degree of orthotropy.

Our sophisticated technology no longer allows us to deal only with the simplified calculations resulting from assumptions of isotropy. These simplified assumptions may lead to inadequate or incorrect results and today's technology requires that we take into account the anisotropy of materials, that is, the differences in elastic properties in various directions [2].

The accurate calculation of stress intensity factors for 3-D cracks has long been recognized as an important computational problem in fracture mechanics. The literature associated with this problem for isotropic materials is quite extensive and a large variety of numerical techniques have been employed to obtain 3-D stress intensity factors. However, there are very few solutions for anisotropic fracture problems in the literature.

The finite element method has become the most commonly used procedure for solving fracture problems. This is due to the relative generality of the approach and existence of a number of commercially available finite element programs that can be used

to generate solutions for 3-D crack geometries. Unfortunately, finite element techniques will not yield suitable results if the severe stress gradient at the crack tip is not properly taken into account. Stress intensity factors determined from local stresses or displacements, require crack tip elements that incorporate the "correct" stress singularity in the asymptotic field. The asymptotic expressions required in the formulation of 3-D crack tip elements are identical to the plane strain asymptotic expressions, i.e., $1/\sqrt{r}$ singularity in stresses, with the same angular variation that is known for plane strain conditions. This asymptotic solution is valid at all points along the crack front, except at the singular point where the crack front intersects the free surface. The most common approach for modeling 3-D cracks using the finite element method is to introduce $1/\sqrt{r}$ singular stress behavior in the crack tip elements by relocating the element mid-side nodes to new locations that cause a singularity in the Jacobian inverse of the geometric transformation. For quadratic elements, this is the so-called "quarter-point technique." This approach results in $1/\sqrt{r}$ stress components in the neighborhood of the crack tip, though it does not ensure the correct θ-dependence. Thus, in practice the quarter-point method requires a highly refined crack tip mesh with wedge elements surrounding the crack tip region. With sufficient mesh refinement, the θ-dependence is adequately approximated. One disadvantage of this approach is the need to create dense, focused, crack tip meshes that cannot be easily generated with conventional automatic mesh generators. When this type of singular element is used, the stress intensity factors along the crack front are determined indirectly by extrapolation of displacements or stresses back to the crack tip and through comparison with the known asymptotic form of the solution.

An alternative approach for computing stress intensity factors using the finite element method is to directly include the stress intensity factors as unknowns in the element displacement field. This can be done by introducing the closed form asymptotic displacement and strain field into the crack tip elements and satisfying compatibility conditions. One of the techniques that utilize this approach is the enriched finite element method. [1]

Enriched finite element method is proved to be accurate in calculating the stress intensity factor of cracks in isotropic materials. The purpose of this study is to extend this special computational technique to the case of anisotropic crack problems.

In this thesis, numerical calculation of stress intensity factors of cracks in anisotropic materials using enriched finite element method is presented. Numerical examples of 3-D straight cracks and 3-D curved cracks are given and a comparison made with the results in which assumption of isotropy is made.

Chapter 2

Crack tip fields in Anisotropic Materials

2.1 Crack tip fields in Anisotropic Materials

The formulation that is used for enriched finite elements will be presented in this chapter. The enriched finite element formulation requires closed form expressions of the displacements and their derivatives. The formulation is given step by step. The treatment will follow references [2,3,4]. However, it should be noted that, there are differences in convention used in these references.

The most general anisotropic form of linear elastic stress-strain relations is given by

$$\varepsilon_{ij} = S_{ij}\sigma_j \tag{2.1}$$

where the components of ε_i and σ_j are given by

$$\varepsilon_x, \varepsilon_y, \varepsilon_z, \gamma_{yz}, \gamma_{zx}, \gamma_{xy} \quad \text{and} \quad \sigma_x, \sigma_y, \sigma_z, \tau_{yz}, \tau_{zx}, \tau_{xy} \tag{2.2}$$

respectively.

By generalized plane deformation condition, the displacements can be written as

$$\begin{aligned} u &= u(x,y) \\ v &= v(x,y) \\ w &= w(x,y) \end{aligned} \tag{2.3}$$

if rigid body rotation about z-axis and rigid body displacements are excluded.

The condition of generalized plane strain assumes that

$$\varepsilon_z = \frac{\partial w_z}{\partial z} = 0 \tag{2.4}$$

and using equation (2.4) ,equation (2.1) gives

$$\sigma_z = -\frac{1}{s_{33}}\left(s_{13}\sigma_x + s_{23}\sigma_y + s_{34}\tau_{yz} + s_{35}\tau_{xz} + s_{36}\tau_{xy}\right) \tag{2.5}$$

Substituting this equation into equation (2.1), the number of independent elastic constants is reduced to fifteen and the strain-stress relation become

$$\begin{bmatrix} \varepsilon_x \\ \varepsilon_y \\ \gamma_{yz} \\ \gamma_{zx} \\ \gamma_{xy} \end{bmatrix} = \begin{bmatrix} M_{11} & M_{12} & M_{14} & M_{15} & M_{16} \\ M_{21} & M_{22} & M_{24} & M_{25} & M_{26} \\ M_{41} & M_{42} & M_{44} & M_{45} & M_{46} \\ M_{51} & M_{52} & M_{54} & M_{55} & M_{56} \\ M_{61} & M_{62} & M_{64} & M_{65} & M_{66} \end{bmatrix} \begin{bmatrix} \sigma_x \\ \sigma_y \\ \tau_{yz} \\ \tau_{zx} \\ \tau_{xy} \end{bmatrix} \tag{2.6}$$

where

$$M_{ij} = s_{ij} - \frac{s_{i3}s_{j3}}{s_{33}} \tag{2.7}$$

It has been shown by Lekthinskii [5], for the generalized plane strain problem, i.e, displacements are invariant in the direction normal to the xy-plane, the elastic field can be represented in terms of three complex analytical functions $\Phi_1(z_1), \Phi_2(z_2), \Phi_3(z_3)$ where $z_j = x + \mu_j y$. μ_j are three distinct complex numbers with positive imaginary parts. These complex numbers are obtained by solving the characteristic equation (2.8), which governs the structure of the stress functions.

Using two Airy-type stress functions, the characteristic equation that is obtained from the equilibrium equations is

$$l_2(\mu)l_4(\mu) - [l_3(\mu)]^2 = 0 \tag{2.8}$$

where

$$
\begin{aligned}
l_2(\mu) &= M_{55}\mu^2 - 2M_{45}\mu + M_{44} \\
l_3(\mu) &= M_{15}\mu^3 - (M_{14} + M_{16})\mu^2 + (M_{25} + M_{46})\mu - M_{24} \\
l_4(\mu) &= M_{11}\mu^4 - 2M_{16}\mu^3 + (2M_{12} + M_{66})\mu^2 - 2M_{26}\mu + M_{22}
\end{aligned} \tag{2.9}
$$

The characteristic equation has six roots, which are complex and will occur in pairs of complex conjugates.

This problem can be formulated in terms of complex analytical functions $\Phi_k(\mu_k)$ as mentioned before. The displacements and stresses can be written in terms of three complex functions,

$$
\begin{aligned}
\sigma_x &= 2\,\mathrm{Re}\{\mu_1^2\Phi_1'(\mu_1) + \mu_2^2\Phi_2'(\mu_2) + \mu_3^2\lambda_3\Phi_3'(\mu_3)\} \\
\sigma_y &= 2\,\mathrm{Re}\{\Phi_1'(\mu_1) + \Phi_2'(\mu_2) + \lambda_3\Phi_3'(\mu_3)\} \\
\tau_{xy} &= -2\,\mathrm{Re}\{\mu_1\Phi_1'(\mu_1) + \mu_2\Phi_2'(\mu_2) + \mu_3\lambda_3\Phi_3'(\mu_3)\} \\
\tau_{xz} &= 2\,\mathrm{Re}\{\mu_1\lambda_1\Phi_1'(\mu_1) + \mu_2\lambda_2\Phi_2'(\mu_2) + \mu_3\Phi_3'(\mu_3)\} \\
\tau_{yz} &= -2\,\mathrm{Re}\{\lambda_1\Phi_1'(\mu_1) + \lambda_2\Phi_2'(\mu_2) + \Phi_3'(\mu_3)\}
\end{aligned} \tag{2.10}
$$

λ_i will be determined by using compatibility equations.

In order to satisfy the compatibility equations, λ_i becomes

$$
\lambda_1 = -\frac{l_3(\mu_1)}{l_2(\mu_1)}, \quad \lambda_2 = -\frac{l_3(\mu_2)}{l_2(\mu_2)}, \quad \lambda_3 = -\frac{l_3(\mu_3)}{l_4(\mu_3)} \tag{2.11}
$$

The displacements;

$$
\begin{aligned}
u &= 2\,\mathrm{Re}\{\sum_{k=1}^{3} p_{1k}\Phi_k(\mu_k)\} \\
v &= 2\,\mathrm{Re}\{\sum_{k=1}^{3} p_{2k}\Phi_k(\mu_k)\} \\
w &= 2\,\mathrm{Re}\{\sum_{k=1}^{3} p_{3k}\Phi_k(\mu_k)\}
\end{aligned} \tag{2.12}
$$

where elements of p_{ij} will be determined by using basic relations between strain and displacements and Equation (2.1)

Writing strains in terms of displacements and combining the Equation (2.1)

$$\begin{aligned} p_{1i} &= M_{11}\mu_i^2 + M_{12} - M_{16}\mu_i + \lambda_i(M_{15}\mu_i - M_{14}) \\ p_{2i} &= M_{12}\mu_i + M_{22}/\mu_i - M_{26} + \lambda_i(M_{25} - M_{24}/\mu_i) \\ p_{3i} &= M_{14}\mu_i + M_{24}/\mu_i - M_{46} + \lambda_i(M_{45} - M_{44}/\mu_i) \end{aligned} \tag{2.13}$$

where i=1,2 and p_{13}, p_{23}, p_{33} are defined separately,

$$\begin{aligned} p_{13} &= \lambda_3(M_{11}\mu_3^2 + M_{12} - M_{16}\mu_3) + M_{15}\mu_3 - M_{14} \\ p_{23} &= \lambda_3(M_{12}\mu_3 + M_{22}/\mu_3 - M_{26}) + M_{25} - M_{24}/\mu_3 \\ p_{33} &= \lambda_3(M_{14}\mu_3 + M_{24}/\mu_3 - M_{46}) + M_{45} - M_{44}/\mu_3 \end{aligned} \tag{2.14}$$

Appropriate selection of a complex function such that satisfies the boundary conditions of the stress free crack faces are as follows.

$$\Phi_k(\mu_k) = B_k\sqrt{\frac{2a\mu_k}{\pi}}, \qquad \Phi_k'(\mu_k) = \frac{B_k\sqrt{a}}{\sqrt{2\pi\mu_k}} \tag{2.15}$$

After substituting Equation (2.15) into Equation (2.16), the constants B_k can be related with stress intensity factors K_I, K_{II}, K_{III} by using conventional definition of stress intensity factors.

$$\begin{aligned} K_I &= \sqrt{2\pi x}\lim_{x\to 0^+}(\sigma_y) \\ K_{II} &= \sqrt{2\pi x}\lim_{x\to 0^+}(\tau_{yx}) \\ K_{III} &= \sqrt{2\pi x}\lim_{x\to 0^+}(\tau_{yz}) \end{aligned} \tag{2.16}$$

$$\begin{bmatrix} K_I \\ K_{II} \\ K_{III} \end{bmatrix} = 2\sqrt{a}\,[N] \begin{bmatrix} B_1 \\ B_2 \\ B_3 \end{bmatrix} \tag{2.17}$$

where

$$[N] = \begin{bmatrix} 1 & 1 & \lambda_3 \\ -\mu_1 & -\mu_2 & -\mu_3\lambda_3 \\ -\lambda_1 & -\lambda_2 & -1 \end{bmatrix} \tag{2.18}$$

hence taking inverse of matrix N;

$$\begin{bmatrix} B_1 \\ B_2 \\ B_3 \end{bmatrix} = \frac{1}{2\sqrt{a}} \frac{1}{\Delta} \begin{bmatrix} \mu_2 - \mu_3\lambda_3\lambda_2 & 1-\lambda_3\lambda_2 & \lambda_3(\mu_2-\mu_3) \\ -\mu_1 + \mu_3\lambda_3\lambda_1 & \lambda_3\lambda_1 - 1 & \lambda_3(\mu_3-\mu_1) \\ \mu_1\lambda_2 - \mu_2\lambda_1 & \lambda_2 - \lambda_1 & \mu_1 - \mu_2 \end{bmatrix} \begin{bmatrix} K_I \\ K_{II} \\ K_{III} \end{bmatrix} \tag{2.19}$$

where

$$\Delta = \mu_2 - \mu_3\lambda_3\lambda_2 - \mu_1 + \mu_1\lambda_3\lambda_2 + \mu_3\lambda_1\lambda_3 - \mu_2\lambda_1\lambda_3 \tag{2.20}$$

Substituting (2.19), (2.13), (2.14), (2.15) into (2.12), yield the closed form expressions for the asymptotic crack tip displacements.

$$\begin{aligned} u &= \sqrt{\frac{2r}{\pi}}\,\mathrm{Re}\{\sum_{k=1}^{3} p_{1k} N_{kl}^{-1} K_I \sqrt{(\cos\theta + \mu_k \sin\theta)}\} \\ v &= \sqrt{\frac{2r}{\pi}}\,\mathrm{Re}\{\sum_{k=1}^{3} p_{2k} N_{kl}^{-1} K_I \sqrt{(\cos\theta + \mu_k \sin\theta)}\} \\ w &= \sqrt{\frac{2r}{\pi}}\,\mathrm{Re}\{\sum_{k=1}^{3} p_{3k} N_{kl}^{-1} K_I \sqrt{(\cos\theta + \mu_k \sin\theta)}\} \end{aligned} \tag{2.21}$$

2.2 Energy Release Rate Formulation:

Strain energy release rate is derived assuming self-similar crack growth. Details concerning derivation of the strain energy release rate formulation will not be presented here. Detailed formulation can be found in Reference [6].

The strain energy release rate can be expressed as

$$G = \frac{1}{2} k^T H^{-1} k \tag{2.22}$$

where

$$k = [K_{II} \quad K_I \quad K_{III}]^T \tag{2.23}$$

$$H = \mathrm{Re}(B) \tag{2.24}$$

where

$$B = iPL^{-1} \tag{2.25}$$

Elements of P matrix are given by equations (2.13) and (2.14).

L is defined separately

$$L = \begin{bmatrix} -\mu_1 & -\mu_2 & -\mu_3\lambda_3 \\ 1 & 1 & \lambda_3 \\ -\lambda_1 & -\lambda_2 & -1 \end{bmatrix} \tag{2.26}$$

After expanding equation (2.22)

$$G = \frac{1}{2}\frac{1}{\Omega}\mathrm{Im}\{(\Gamma_1(1-\lambda_3\lambda_2)+\Gamma_2(-1+\lambda_3\lambda_1)+\Gamma_3(\lambda_2+\lambda_1))K_{II} + (\Gamma_1(\mu_2-\mu_3\lambda_3\lambda_2) + \Gamma_2(-\mu_1+\lambda_1\mu_3\lambda_3)+\Gamma_3(\lambda_2\mu_1-\lambda_1\mu_2))K_I + (\Gamma_1\lambda_3(\mu_2-\mu_3)+\Gamma_2\lambda_3(\mu_3-\mu_1)+\Gamma_3(\mu_1-\mu_2))K_{III}\} \tag{2.27}$$

where

$$\begin{aligned} \Gamma_1 &= K_{II}p_{11}+K_I p_{21}+K_{III}p_{31} \\ \Gamma_2 &= K_{II}p_{12}+K_I p_{22}+K_{III}p_{32} \\ \Gamma_3 &= K_{II}p_{13}+K_I p_{23}+K_{III}p_{33} \end{aligned} \tag{2.28}$$

$$\Omega = -\mu_2 + \mu_3\lambda_3\lambda_2 + \mu_1 - \mu_1\lambda_3\lambda_2 - \mu_3\lambda_1\lambda_3 + \mu_2\lambda_1\lambda_3 \tag{2.29}$$

Chapter3

Enriched Finite Element Formulation

3.1 Introduction

The enriched finite element formulation is presented in this chapter. The enriched element asymptotic displacements terms are given explicitly. Formation of the enriched element stiffness matrix is described in detail. In the following treatment, the details closely follow Reference [1].

3.2 Enriched Element Displacements

The enriched crack tip elements as formulated by Benzley [10] for 2-D problems, contain the closed form asymptotic field for crack tip displacements, in addition to the usual polynomial interpolation function. Thus, the enriched element displacements u, v, and w take the form [11],

$$u(\xi,\eta,\rho)=\sum_{j=1}^{r}N_j(\xi,\eta,\rho)u_j+Z_0(\xi,\eta,\rho)\{K_I(\Gamma)F_1(\xi,\eta,\rho)+K_{II}(\Gamma)G_1(\xi,\eta,\rho)+K_{III}(\Gamma)H_1(\xi,\eta,\rho)\} \tag{3.1}$$

$$v(\xi,\eta,\rho)=\sum_{j=1}^{r}N_j(\xi,\eta,\rho)v_j+Z_0(\xi,\eta,\rho)\{K_I(\Gamma)F_2(\xi,\eta,\rho)+K_{II}(\Gamma)G_2(\xi,\eta,\rho)+K_{III}(\Gamma)H_2(\xi,\eta,\rho)\} \tag{3.2}$$

$$w(\xi,\eta,\rho)=\sum_{j=1}^{r}N_j(\xi,\eta,\rho)w_j+Z_0(\xi,\eta,\rho)\{K_I(\Gamma)F_3(\xi,\eta,\rho)+K_{II}(\Gamma)G_3(\xi,\eta,\rho)+K_{III}(\Gamma)H_3(\xi,\eta,\rho)\} \tag{3.3}$$

In equations (3.1)-(3.3) u_j, v_j and w_j represent the r unknown nodal displacements and $N_j(\xi,\eta,\rho)$ are the conventional element shape functions in terms of the element's local coordinates. $K_I(\Gamma), K_{II}(\Gamma), K_{III}(\Gamma)$ represent the mode I, II and III stress intensity factors varying along the crack front defined by the interpolation functions $N_i(\Gamma)$.

$$K_I(\Gamma)=\sum_{i=1}^{s}N_i(\Gamma)K_I^i\ ,\ K_{II}(\Gamma)=\sum_{i=1}^{s}N_i(\Gamma)K_{II}^i\ ,\ K_{III}(\Gamma)=\sum_{i=1}^{s}N_i(\Gamma)K_{III}^i \tag{3.4}$$

where K_I^i, K_{II}^i, and K_{III}^i are the unknown stress intensity factors at the ith crack tip node in the enriched element (see Figure 1). In most cases, $N_i(\Gamma)$ will be the element shape function along the element edge coinciding with the crack front. Written in terms of the crack tip nodal coordinates x_i, y_i, z_i, the crack front is defined by

$$x=\sum_{i=1}^{s}N_i(\Gamma)x_i,\quad y=\sum_{i=1}^{s}N_i(\Gamma)y_i,\quad z=\sum_{i=1}^{s}N_i(\Gamma)z_i \tag{3.5}$$

Thus, $\Gamma=\xi$, $\Gamma=\eta$, or $\Gamma=\rho$, depending on which edge of the element touches the crack front. For example, for a 20-noded hexahedron that has a crack front located on the edge defined by $\eta=-1, \rho=-1$, with $(-1\le\xi\le 1)$,

$$K_I(\Gamma)=K_I(\xi)=\tfrac{1}{2}(-\xi+\xi^2)K_I^1+(1-\xi^2)K_I^2+\tfrac{1}{2}(\xi+\xi^2)K_I^3 \tag{3.6}$$

In Equation (3.6), K_I^1, K_I^2, K_I^3 are the mode I stress intensity factors at the nodes located at $\xi=-1, \xi=0, \xi=1$, respectively. The mode II and mode III stress intensity factors would be defined in a similar manner.

3.3 Asymptotic Terms

Figure 1 depicts a cubic enriched element (32-noded hexahedron) with four nodes along the crack front. Thus, for the cubic element, the summation over the stress intensity

factor terms in Equation (3.4) has an upper limit s = 4 (two corner and two mid-side nodes) and for the quadratic element s = 3 (two corner and one mid-side node). The cubic hexahedron therefore has 108 degrees of freedom (96 displacements and 12 stress intensity factors). In a likewise manner, the enriched quadratic hexahedron has 69 dof's (60 displacements and 9 stress intensity factors). The functions F_i, G_i, H_i in (3.1) – (3.3) are given by

$$F_i(\xi,\eta,\rho) = f_i(\xi,\eta,\rho) - \sum_{j=1}^{r} N_j(\xi,\eta,\rho) f_{ij} \tag{3.7}$$

$$G_i(\xi,\eta,\rho) = g_i(\xi,\eta,\rho) - \sum_{j=1}^{r} N_j(\xi,\eta,\rho) g_{ij} \tag{3.8}$$

$$H_i(\xi,\eta,\rho) = h_i(\xi,\eta,\rho) - \sum_{j=1}^{r} N_j(\xi,\eta,\rho) h_{ij} \tag{3.9}$$

In (3.7)- (3.9), $f_i, g_i, h_i (i = 1,2,3)$ contain the asymptotic displacement functions that are coefficients of the mode I, II and III stress intensity factors transformed to the global coordinate system. The terms $f_{1j}, g_{1j}, h_{1j}, f_{2j}, g_{2j}, h_{2j}, f_{3j}, g_{3j}, h_{3j}$ in (3.7)- (3.9) are simply constants computed from the f_i, g_i, h_i functions evaluated at the jth node in the element. For a homogeneous, anisotropic material, the asymptotic crack tip displacements in the local (primed) coordinate system are can be written as

$$\bar{u} = K_I \bar{f}_1 + K_{II} \bar{g}_1 + K_{III} \bar{h}_1 \tag{3.10}$$

$$\bar{v} = K_I \bar{f}_2 + K_{II} \bar{g}_2 + K_{III} \bar{h}_2 \tag{3.11}$$

$$\bar{w} = K_I \bar{f}_3 + K_{II} \bar{g}_3 + K_{III} \bar{h}_3 \tag{3.12}$$

where

$$\overline{f_1} = \sqrt{\frac{2r}{\pi}}\,\mathrm{Re}\{p_{11}N_{11}{}^{-1}\sqrt{\cos(\theta)+\mu_1\sin(\theta)} + p_{12}N_{21}{}^{-1}\sqrt{\cos(\theta)+\mu_2\sin(\theta)} + p_{13}N_{31}{}^{-1}\sqrt{\cos(\theta)+\mu_3\sin(\theta)}\} \tag{3.13}$$

$$\overline{g_1} = \sqrt{\frac{2r}{\pi}}\,\mathrm{Re}\{p_{11}N_{12}{}^{-1}\sqrt{\cos(\theta)+\mu_1\sin(\theta)} + p_{12}N_{22}{}^{-1}\sqrt{\cos(\theta)+\mu_2\sin(\theta)} + p_{13}N_{32}{}^{-1}\sqrt{\cos(\theta)+\mu_3\sin(\theta)}\} \tag{3.14}$$

$$\overline{h_1} = \sqrt{\frac{2r}{\pi}}\,\mathrm{Re}\{p_{11}N_{13}{}^{-1}\sqrt{\cos(\theta)+\mu_1\sin(\theta)} + p_{12}N_{23}{}^{-1}\sqrt{\cos(\theta)+\mu_2\sin(\theta)} + p_{13}N_{33}{}^{-1}\sqrt{\cos(\theta)+\mu_3\sin(\theta)}\} \tag{3.15}$$

$$\overline{f_2} = \sqrt{\frac{2r}{\pi}}\,\mathrm{Re}\{p_{21}N_{11}{}^{-1}\sqrt{\cos(\theta)+\mu_1\sin(\theta)} + p_{22}N_{21}{}^{-1}\sqrt{\cos(\theta)+\mu_2\sin(\theta)} + p_{23}N_{31}{}^{-1}\sqrt{\cos(\theta)+\mu_3\sin(\theta)}\} \tag{3.16}$$

$$\overline{g_2} = \sqrt{\frac{2r}{\pi}}\,\mathrm{Re}\{p_{21}N_{12}{}^{-1}\sqrt{\cos(\theta)+\mu_1\sin(\theta)} + p_{22}N_{22}{}^{-1}\sqrt{\cos(\theta)+\mu_2\sin(\theta)} + p_{23}N_{32}{}^{-1}\sqrt{\cos(\theta)+\mu_3\sin(\theta)}\} \tag{3.17}$$

$$\overline{h_2} = \sqrt{\frac{2r}{\pi}}\,\mathrm{Re}\{p_{21}N_{13}{}^{-1}\sqrt{\cos(\theta)+\mu_1\sin(\theta)} + p_{22}N_{23}{}^{-1}\sqrt{\cos(\theta)+\mu_2\sin(\theta)} + p_{23}N_{33}{}^{-1}\sqrt{\cos(\theta)+\mu_3\sin(\theta)}\} \tag{3.18}$$

$$\overline{f_3} = \sqrt{\frac{2r}{\pi}}\,\mathrm{Re}\{p_{31}N_{11}{}^{-1}\sqrt{\cos(\theta)+\mu_1\sin(\theta)} + p_{32}N_{21}{}^{-1}\sqrt{\cos(\theta)+\mu_2\sin(\theta)} + p_{33}N_{31}{}^{-1}\sqrt{\cos(\theta)+\mu_3\sin(\theta)}\} \tag{3.19}$$

$$\overline{g_3} = \sqrt{\frac{2r}{\pi}}\,\mathrm{Re}\{p_{31}N_{12}{}^{-1}\sqrt{\cos(\theta)+\mu_1\sin(\theta)} + p_{32}N_{22}{}^{-1}\sqrt{\cos(\theta)+\mu_2\sin(\theta)} + p_{33}N_{32}{}^{-1}\sqrt{\cos(\theta)+\mu_3\sin(\theta)}\} \tag{3.20}$$

$$\bar{h}_3 = \sqrt{\frac{2r}{\pi}}\,\mathrm{Re}\{p_{31}N_{13}^{-1}\sqrt{\cos(\theta)+\mu_1\sin(\theta)} + p_{32}N_{23}^{-1}\sqrt{\cos(\theta)+\mu_2\sin(\theta)} + p_{33}N_{33}^{-1}\sqrt{\cos(\theta)+\mu_3\sin(\theta)}\} \tag{3.21}$$

In (3.13)-(3.21), the components p_{ij} and the components of N matrix inverse are derive from material constants which changes with the local crack tip coordinate system and were defined in the previous section where r and θ are measured locally from the crack front as shown in Figure 1. The relationships between the local crack tip displacement components $\bar{u}_i$, Equations (3.10)-(3.21), and the global displacements u_i, are found through the usual vector transformations. Using index notation

$$u_i = a_{ji}\bar{u}_j \tag{3.22}$$

where a_{ji} represents the direction cosines between the primed axes and the global axes in Figure 1, i.e., $a_{11} = \cos(x',x)$, $a_{12} = \cos(x',y)$, $a_{13} = \cos(x',z)$, etc. Transforming the asymptotic displacements in Equation (3.10)-(3.12) to global coordinates yields the following terms for f_i, g_i, and h_i in (3.7) – (3.9)

$$f_i = \bar{f}_1 a_{1i} + \bar{f}_2 a_{2i} + \bar{f}_3 a_{3i} \tag{3.23}$$

$$g_i = \bar{g}_1 a_{1i} + \bar{g}_2 a_{2i} + \bar{g}_3 a_{3i} \tag{3.24}$$

$$h_i = \bar{h}_1 a_{1i} + \bar{h}_2 a_{2i} + \bar{h}_3 a_{3i} \tag{3.25}$$

It should be noted that the direction cosines used to perform the local-to-global transformations are in general different at every point in the enriched element. In addition, for element coordinate values of ξ, η, ρ located at the element nodes, the displacements are simply given by the leading terms in Equations (3.1)-(3.3), since

F_i, G_i, and H_i, Equations (3.7)-(3.9), are identically zero at these points. Also, it should be mentioned that, the cosines used for local-to-global coordinate transformations are also used to transform the global material properties to local coordinate material properties. For example, in the case of a curved crack, the local crack tip coordinates change along the crack front. The material properties also change with respect to the new local crack tip coordinate system. This tensor transformation of the compliance matrix is straightforward and explained in detail in Reference [5].

3.4 Zeroing Functions for Transition Elements

Since the enriched crack tip element contains non-polynomial analytic terms, displacement compatibility cannot automatically be ensured on surfaces between enriched elements and neighboring regular elements that do not contain the asymptotic terms. To enforce displacement compatibility between all elements, transition elements should be used between the fully enriched crack tip elements and the regular elements. Figure 2 shows the location of these transition elements, with respect to the enriched crack tip elements, along the front of a semi-elliptic surface crack. For the crack tip elements, $Z_0(\xi,\eta,\rho)$ in (3.1) – (3.3) is a constant equal to 1. For transition elements, $Z_0(\xi,\eta,\rho)$ represents a function that has a value of 1 where the transition element contacts the fully enriched crack tip element and a value of 0 where the element touches a regular element. Various forms for Z_0 were tested in [12] using 2-D elements, with the conclusion that although it is important to include transition elements in the enriched element formulation, the specific form of the "zeroing" function is of relatively minor importance. Thus, in this study linear functions were used for the transition elements. The relevant details for other 3-D transition elements are given in [11]. Examples of linear

zeroing functions and detailed explanation of importance of these functions can be found in [1].

3.5 Enriched Element Stiffness Matrix

With displacements given by Equations (3.1)-(3.3), it is possible to develop the usual displacement based finite element equations for an elastic continuum. Details concerning the finite element formulation, assembly of the global stiffness matrix, and solution of the system of equations are given in a number of books on this topic, e.g., [13]. Of particular importance in this study is the evaluation of the enriched element stiffness matrix, i.e.,

$$[K]=\int_{-1}^{1}\int_{-1}^{1}\int_{-1}^{1}[B]^T[E][B]\det \boldsymbol{J}\,d\xi\,d\eta\,d\rho \tag{3.26}$$

where $\boldsymbol{J}$ is the Jacobian, $[B]$ the strain shape function matrix, and $[E]$ the material property matrix. Calculation of $[B]$ requires evaluation of derivatives of Equations (3.1)-(3.3) that include derivatives of the analytic terms as well as the shape functions. The required derivatives of the displacement field with respect to x, y, and z, can be found by simply using the chain rule for differentiation or in matrix form, the inverse of the Jacobian, i.e.,

$$\begin{Bmatrix}\frac{\partial u}{\partial x}\\ \frac{\partial u}{\partial y}\\ \frac{\partial u}{\partial z}\end{Bmatrix}=[J]^{-1}\begin{Bmatrix}\frac{\partial u}{\partial \xi}\\ \frac{\partial u}{\partial \eta}\\ \frac{\partial u}{\partial \rho}\end{Bmatrix},\quad \begin{Bmatrix}\frac{\partial v}{\partial x}\\ \frac{\partial v}{\partial y}\\ \frac{\partial v}{\partial z}\end{Bmatrix}=[J]^{-1}\begin{Bmatrix}\frac{\partial v}{\partial \xi}\\ \frac{\partial v}{\partial \eta}\\ \frac{\partial v}{\partial \rho}\end{Bmatrix},\quad \begin{Bmatrix}\frac{\partial w}{\partial x}\\ \frac{\partial w}{\partial y}\\ \frac{\partial w}{\partial z}\end{Bmatrix}=[J]^{-1}\begin{Bmatrix}\frac{\partial w}{\partial \xi}\\ \frac{\partial w}{\partial \eta}\\ \frac{\partial w}{\partial \rho}\end{Bmatrix} \tag{3.27}$$

The explicit expressions for the derivatives of displacements with respect to (ξ,η,ρ) on the right hand side of(3.27), are obtained by directly differentiating(3.1)-(3.3), e.g.,

$$\frac{\partial u(\xi,\eta,\rho)}{\partial \xi} = \sum_{j=1}^{r} \frac{\partial N_j}{\partial \xi} u_j + \sum_{i=1}^{s} \left[\left\{ \frac{\partial Z_0}{\partial \xi} F_1 + Z_0 \frac{\partial F_1}{\partial \xi} \right\} N_i(\Gamma) + Z_0 F_1 \frac{\partial N_i(\Gamma)}{\partial \xi} \right] K_I^i$$
$$+ \sum_{i=1}^{s} \left[\left\{ \frac{\partial Z_0}{\partial \xi} G_1 + Z_0 \frac{\partial G_1}{\partial \xi} \right\} N_i(\Gamma) + Z_0 G_1 \frac{\partial N_i(\Gamma)}{\partial \xi} \right] K_{II}^i \qquad (3.28)$$
$$+ \sum_{i=1}^{s} \left[\left\{ \frac{\partial Z_0}{\partial \xi} H_1 + Z_0 \frac{\partial H_1}{\partial \xi} \right\} N_i(\Gamma) + Z_0 H_1 \frac{\partial N_i(\Gamma)}{\partial \xi} \right] K_{III}^i$$

$$\frac{\partial u(\xi,\eta,\rho)}{\partial \eta} = \sum_{j=1}^{r} \frac{\partial N_j}{\partial \eta} u_j + \sum_{i=1}^{s} \left[\left\{ \frac{\partial Z_0}{\partial \eta} F_1 + Z_0 \frac{\partial F_1}{\partial \eta} \right\} N_i(\Gamma) + Z_0 F_1 \frac{\partial N_i(\Gamma)}{\partial \eta} \right] K_I^i$$
$$+ \sum_{i=1}^{s} \left[\left\{ \frac{\partial Z_0}{\partial \eta} G_1 + Z_0 \frac{\partial G_1}{\partial \eta} \right\} N_i(\Gamma) + Z_0 G_1 \frac{\partial N_i(\Gamma)}{\partial \eta} \right] K_{II}^i \qquad (3.29)$$
$$+ \sum_{i=1}^{s} \left[\left\{ \frac{\partial Z_0}{\partial \eta} H_1 + Z_0 \frac{\partial H_1}{\partial \eta} \right\} N_i(\Gamma) + Z_0 H_1 \frac{\partial N_i(\Gamma)}{\partial \eta} \right] K_{III}^i$$

$$\frac{\partial u(\xi,\eta,\rho)}{\partial \rho} = \sum_{j=1}^{r} \frac{\partial N_j}{\partial \rho} u_j + \sum_{i=1}^{s} \left[\left\{ \frac{\partial Z_0}{\partial \rho} F_1 + Z_0 \frac{\partial F_1}{\partial \rho} \right\} N_i(\Gamma) + Z_0 F_1 \frac{\partial N_i(\Gamma)}{\partial \rho} \right] K_I^i$$
$$+ \sum_{i=1}^{s} \left[\left\{ \frac{\partial Z_0}{\partial \rho} G_1 + Z_0 \frac{\partial G_1}{\partial \rho} \right\} N_i(\Gamma) + Z_0 G_1 \frac{\partial N_i(\Gamma)}{\partial \rho} \right] K_{II}^i \qquad (3.30)$$
$$+ \sum_{i=1}^{s} \left[\left\{ \frac{\partial Z_0}{\partial \rho} H_1 + Z_0 \frac{\partial H_1}{\partial \rho} \right\} N_i(\Gamma) + Z_0 H_1 \frac{\partial N_i(\Gamma)}{\partial \rho} \right] K_{III}^i$$

Derivatives of displacements v and w with respect to (ξ,η,ρ) in (3.27) are obtained in a similar manner. Equations (3.28)-(3.30) clearly show that each derivative term has a total of r factors containing the unknown nodal displacements u_j, as well as $3s$ unknown stress intensity factors. All derivatives of Z_0 are zero for enriched crack tip elements. For transition elements, these derivatives are simple functions of (ξ,η,ρ). Details can be found in reference [1]

Derivatives of F_i, G_i, and H_i in the expressions (3.28) -(3.30) and related derivatives of v and w, require differentiation of (3.7)- (3.9) with respect to (ξ,η,ρ). This in turn means differentiation of Equations (3.23)-(3.25). These derivatives are determined through successive use of the chain rule. Derivatives of the primed coordinates with

respect to the global coordinates, e.g., $\frac{\partial x'}{\partial x}, \frac{\partial y'}{\partial x}, \frac{\partial z'}{\partial x}, \cdots$, can be expressed in terms of the direction cosines, a_{ij}, i.e., using index notation $\frac{\partial x_i'}{\partial x_j} = a_{ij}$. Referring to Equation (3.23), the derivatives of f_1 with respect to the local coordinates x', y', z' are

$$\frac{\partial f_1}{\partial x'} = \frac{\partial \overline{f}_1}{\partial x'} a_{11} + \frac{\partial \overline{f}_2}{\partial x'} a_{21} + \frac{\partial \overline{f}_3}{\partial x'} a_{31} \tag{3.31}$$

$$\frac{\partial f_1}{\partial y'} = \frac{\partial \overline{f}_1}{\partial y'} a_{11} + \frac{\partial \overline{f}_2}{\partial y'} a_{21} + \frac{\partial \overline{f}_3}{\partial y'} a_{31} \tag{3.32}$$

$$\frac{\partial f_1}{\partial z'} = \frac{\partial \overline{f}_1}{\partial z'} a_{11} + \frac{\partial \overline{f}_2}{\partial z'} a_{21} + \frac{\partial \overline{f}_3}{\partial z'} a_{31} \tag{3.33}$$

Ultimately, differentiation of the F_i, G_i, and H_i terms in(3.28)-(3.30), involves differentiation of the asymptotic displacement expressions, (3.13)-(3.21), with respect to the primed coordinates:

Derivatives with respect to x':

$$\frac{\partial \overline{f}_1}{\partial x'} = \sqrt{\frac{1}{2\pi r}} \operatorname{Re}\left\{ \frac{p_{11} N_{11}^{-1}}{\sqrt{\cos(\theta) + \mu_1 \sin(\theta)}} + \frac{p_{12} N_{21}^{-1}}{\sqrt{\cos(\theta) + \mu_2 \sin(\theta)}} + \frac{p_{13} N_{31}^{-1}}{\sqrt{\cos(\theta) + \mu_3 \sin(\theta)}} \right\} \tag{3.34}$$

$$\frac{\partial \overline{g}_1}{\partial x'} = \sqrt{\frac{1}{2\pi r}} \operatorname{Re}\left\{ \frac{p_{11} N_{12}^{-1}}{\sqrt{\cos(\theta) + \mu_1 \sin(\theta)}} + \frac{p_{12} N_{22}^{-1}}{\sqrt{\cos(\theta) + \mu_2 \sin(\theta)}} + \frac{p_{13} N_{32}^{-1}}{\sqrt{\cos(\theta) + \mu_3 \sin(\theta)}} \right\} \tag{3.35}$$

$$\frac{\partial \overline{h}_1}{\partial x'} = \sqrt{\frac{1}{2\pi r}} \operatorname{Re}\left\{ \frac{p_{11} N_{13}^{-1}}{\sqrt{\cos(\theta) + \mu_1 \sin(\theta)}} + \frac{p_{12} N_{23}^{-1}}{\sqrt{\cos(\theta) + \mu_2 \sin(\theta)}} + \frac{p_{13} N_{33}^{-1}}{\sqrt{\cos(\theta) + \mu_3 \sin(\theta)}} \right\} \tag{3.36}$$

$$\frac{\partial \overline{f}_2}{\partial x'} = \sqrt{\frac{1}{2\pi r}} \operatorname{Re}\left\{ \frac{p_{21} N_{11}^{-1}}{\sqrt{\cos(\theta) + \mu_1 \sin(\theta)}} + \frac{p_{22} N_{21}^{-1}}{\sqrt{\cos(\theta) + \mu_2 \sin(\theta)}} + \frac{p_{23} N_{31}^{-1}}{\sqrt{\cos(\theta) + \mu_3 \sin(\theta)}} \right\} \tag{3.37}$$

$$\frac{\partial \overline{g_2}}{\partial x'} = \sqrt{\frac{1}{2\pi r}}\,\mathrm{Re}\{\frac{p_{21}N_{12}^{-1}}{\sqrt{\cos(\theta)+\mu_1\sin(\theta)}} + \frac{p_{22}N_{22}^{-1}}{\sqrt{\cos(\theta)+\mu_2\sin(\theta)}} + \frac{p_{23}N_{32}^{-1}}{\sqrt{\cos(\theta)+\mu_3\sin(\theta)}}\} \quad (3.38)$$

$$\frac{\partial \overline{h_2}}{\partial x'} = \sqrt{\frac{1}{2\pi r}}\,\mathrm{Re}\{\frac{p_{21}N_{13}^{-1}}{\sqrt{\cos(\theta)+\mu_1\sin(\theta)}} + \frac{p_{22}N_{23}^{-1}}{\sqrt{\cos(\theta)+\mu_2\sin(\theta)}} + \frac{p_{23}N_{33}^{-1}}{\sqrt{\cos(\theta)+\mu_3\sin(\theta)}}\} \quad (3.39)$$

$$\frac{\partial \overline{f_3}}{\partial x'} = \sqrt{\frac{1}{2\pi r}}\,\mathrm{Re}\{\frac{p_{31}N_{11}^{-1}}{\sqrt{\cos(\theta)+\mu_1\sin(\theta)}} + \frac{p_{32}N_{21}^{-1}}{\sqrt{\cos(\theta)+\mu_2\sin(\theta)}} + \frac{p_{33}N_{31}^{-1}}{\sqrt{\cos(\theta)+\mu_3\sin(\theta)}}\} \quad (3.40)$$

$$\frac{\partial \overline{g_3}}{\partial x'} = \sqrt{\frac{1}{2\pi r}}\,\mathrm{Re}\{\frac{p_{31}N_{12}^{-1}}{\sqrt{\cos(\theta)+\mu_1\sin(\theta)}} + \frac{p_{32}N_{22}^{-1}}{\sqrt{\cos(\theta)+\mu_2\sin(\theta)}} + \frac{p_{33}N_{32}^{-1}}{\sqrt{\cos(\theta)+\mu_3\sin(\theta)}}\} \quad (3.41)$$

$$\frac{\partial \overline{h_3}}{\partial x'} = \sqrt{\frac{1}{2\pi r}}\,\mathrm{Re}\{\frac{p_{31}N_{13}^{-1}}{\sqrt{\cos(\theta)+\mu_1\sin(\theta)}} + \frac{p_{32}N_{23}^{-1}}{\sqrt{\cos(\theta)+\mu_2\sin(\theta)}} + \frac{p_{33}N_{33}^{-1}}{\sqrt{\cos(\theta)+\mu_3\sin(\theta)}}\} \quad (3.42)$$

Derivatives with respect to y':

$$\frac{\partial \overline{f_1}}{\partial y'} = \sqrt{\frac{1}{2\pi r}}\,\mathrm{Re}\{\frac{p_{11}N_{11}^{-1}}{\sqrt{\cos(\theta)+\mu_1\sin(\theta)}}\mu_1 + \frac{p_{12}N_{21}^{-1}}{\sqrt{\cos(\theta)+\mu_2\sin(\theta)}}\mu_2 + \frac{p_{13}N_{31}^{-1}}{\sqrt{\cos(\theta)+\mu_3\sin(\theta)}}\mu_3\} \quad (3.43)$$

$$\frac{\partial \overline{g_1}}{\partial y'} = \sqrt{\frac{1}{2\pi r}}\,\mathrm{Re}\{\frac{p_{11}N_{12}^{-1}}{\sqrt{\cos(\theta)+\mu_1\sin(\theta)}}\mu_1 + \frac{p_{12}N_{22}^{-1}}{\sqrt{\cos(\theta)+\mu_2\sin(\theta)}}\mu_2 + \frac{p_{13}N_{32}^{-1}}{\sqrt{\cos(\theta)+\mu_3\sin(\theta)}}\mu_3\} \quad (3.44)$$

$$\frac{\partial \overline{h_1}}{\partial y'} = \sqrt{\frac{1}{2\pi r}}\,\mathrm{Re}\{\frac{p_{11}N_{13}^{-1}}{\sqrt{\cos(\theta)+\mu_1\sin(\theta)}}\mu_1 + \frac{p_{12}N_{23}^{-1}}{\sqrt{\cos(\theta)+\mu_2\sin(\theta)}}\mu_2 + \frac{p_{13}N_{33}^{-1}}{\sqrt{\cos(\theta)+\mu_3\sin(\theta)}}\mu_3\} \quad (3.45)$$

$$\frac{\partial \overline{f_2}}{\partial y'} = \sqrt{\frac{1}{2\pi r}}\,\mathrm{Re}\{\frac{p_{21}N_{11}^{-1}}{\sqrt{\cos(\theta)+\mu_1\sin(\theta)}}\mu_1 + \frac{p_{22}N_{21}^{-1}}{\sqrt{\cos(\theta)+\mu_2\sin(\theta)}}\mu_2 + \frac{p_{23}N_{31}^{-1}}{\sqrt{\cos(\theta)+\mu_3\sin(\theta)}}\mu_3\} \quad (3.46)$$

$$\frac{\partial \overline{g_2}}{\partial y'} = \sqrt{\frac{1}{2\pi r}}\,\mathrm{Re}\{\frac{p_{21}N_{12}^{-1}}{\sqrt{\cos(\theta)+\mu_1\sin(\theta)}}\mu_1 + \frac{p_{22}N_{22}^{-1}}{\sqrt{\cos(\theta)+\mu_2\sin(\theta)}}\mu_2 + \frac{p_{23}N_{32}^{-1}}{\sqrt{\cos(\theta)+\mu_3\sin(\theta)}}\mu_3\} \quad (3.47)$$

$$\frac{\partial \bar{h}_2}{\partial y'} = \sqrt{\frac{1}{2\pi r}}\,\mathrm{Re}\left\{\frac{p_{21}N_{13}^{-1}}{\sqrt{\cos(\theta)+\mu_1\sin(\theta)}}\mu_1 + \frac{p_{22}N_{23}^{-1}}{\sqrt{\cos(\theta)+\mu_2\sin(\theta)}}\mu_2 + \frac{p_{23}N_{33}^{-1}}{\sqrt{\cos(\theta)+\mu_3\sin(\theta)}}\mu_3\right\} \quad (3.48)$$

$$\frac{\partial \bar{f}_3}{\partial y'} = \sqrt{\frac{1}{2\pi r}}\,\mathrm{Re}\left\{\frac{p_{31}N_{11}^{-1}}{\sqrt{\cos(\theta)+\mu_1\sin(\theta)}}\mu_1 + \frac{p_{32}N_{21}^{-1}}{\sqrt{\cos(\theta)+\mu_2\sin(\theta)}}\mu_2 + \frac{p_{33}N_{31}^{-1}}{\sqrt{\cos(\theta)+\mu_3\sin(\theta)}}\mu_3\right\} \quad (3.49)$$

$$\frac{\partial \bar{g}_3}{\partial y'} = \sqrt{\frac{1}{2\pi r}}\,\mathrm{Re}\left\{\frac{p_{31}N_{12}^{-1}}{\sqrt{\cos(\theta)+\mu_1\sin(\theta)}}\mu_1 + \frac{p_{32}N_{22}^{-1}}{\sqrt{\cos(\theta)+\mu_2\sin(\theta)}}\mu_2 + \frac{p_{33}N_{32}^{-1}}{\sqrt{\cos(\theta)+\mu_3\sin(\theta)}}\mu_3\right\} \quad (3.50)$$

$$\frac{\partial \bar{h}_3}{\partial y'} = \sqrt{\frac{1}{2\pi r}}\,\mathrm{Re}\left\{\frac{p_{31}N_{13}^{-1}}{\sqrt{\cos(\theta)+\mu_1\sin(\theta)}}\mu_1 + \frac{p_{32}N_{23}^{-1}}{\sqrt{\cos(\theta)+\mu_2\sin(\theta)}}\mu_2 + \frac{p_{33}N_{33}^{-1}}{\sqrt{\cos(\theta)+\mu_3\sin(\theta)}}\mu_3\right\} \quad (3.51)$$

Expressions (3.34)-(3.51) introduce the well-known $\sqrt{r}$ singularity into the strain shape function matrix $[B]$. Since the local asymptotic displacement field is independent of z', all derivatives with respect to the local z' coordinates are zero.

Special cases and a detailed explanation of the formation of the stiffness matrix for enriched finite elements can be found in [1].

3.6 Integration of Enriched Elements

Some special care must be taken to accurately evaluate the integral in (3.26) during formation of the element stiffness matrix. For regular elements, this integral is evaluated using n^3 Gaussian quadrature points [13]. For example, a regular cubic hexahedron would have 4x4x4 Gaussian integration points. Since the enriched and transition elements contain non-polynomial analytic terms, these elements generally require higher order integration than the regular elements, e.g., 30x30x30. Integration convergence should be checked to ensure the most accurate stress intensity factor results. Standard integration in

the element's natural (ξ, η, ρ) coordinates is the simplest approach. In Chapter 4, the effect of integration order is discussed.

Chapter 4

Example Calculations

4.1 Introduction

A new anisotropic version of the finite element program, FRAC3D, was developed for general three-dimensional fracture analysis based on the preceding enriched finite element formulation. A previous version of FRAC3D is suitable for analyses of three-dimensional fracture problems in isotropic materials [1]. Most details concerning element stiffness matrix formation, calculation of consistent nodal forces, assembly, solution, and implementation of boundary conditions are described by Ayhan in [11]. Numerical examples are presented that demonstrate the application of three-dimensional enriched finite elements for selected homogeneous, anisotropic, three-dimensional fracture problems.

4.2 Edge Cracked Bar where Crack is Aligned with Orthotropy Axis

Figure 3 depicts the geometry and Figure 4 depicts two meshes used to model a solid bar containing a straight through edge crack subjected to remote uniaxial stress σ_0. The purpose of this simple example is to demonstrate the accuracy of the enriched element approach for a problem with a known solution. However, these solutions exist only for orthotropic materials and the crack must be aligned with the principal orthotropy axis. In other words, the α in the Figure 3 is zero. The α is defined in Figure 3. The complete bar is shown. The crack is not visible in these mesh models, because the symmetry conditions were not used. The reason for this is so that these results can be

directly compared with a related case, where there is no symmetry due to material orientation.

The ratio of the crack length a to width of the bar h is a/h = 0.5. Plane strain conditions were enforced on the 3-D models by constraining out-of-plane displacements on the front and back faces. For comparison, a very accurate integral equation solution to this problem is given in [7], i.e., $K_{IR} = 2.7199\sigma_0\sqrt{\pi a}$, for an orthotropic material with the following properties: $E_x = 24.75E+6$, $G_{xy} = 0.7E+6$, $E_y = 8.0E+6$, $\nu_{xy} = 0.1114$. Since the analysis given in Reference [7] was for 2-D, the material is assumed to be transversely isotropic. The fifth independent constant assumed for 3-D calculation, necessary was $\nu_{yz} = 0.4$

Figure 5 contains the normalized stress intensity factors computed for the two meshes shown in Fig 3. In both models, four quadratic elements were used in the thickness direction. In the first model, designated SEL=0.25a, the Size of Edge Length measured perpendicular to the crack front, is 0.25a. In the refined model, designated SEL=0.025a, this dimension is 10 times smaller.

The normalized stress intensity factors are presented in Figure 3. The results are normalized with the reference stress intensity factor in Reference [7]. It can be seen in Figure 3, mesh refinement does not have significant effect on convergence. The normalized stress intensity factors for two different meshes almost coincide. As Figure 5 shows, integration order has a far greater impact on convergence than mesh refinement. Thus, while a regular quadratic hexahedron can be integrated with 3x3x3 Gaussian quadrature points, enriched elements should be integrated using substantially more

points. Increasing the number of integration points results in a converged solution for the stress intensity factors. However, convergence to the "correct" solution also requires successive mesh refinement, as is always the case in traditional finite element analysis. The unrefined mesh with SEL=0.25 yields an error of 0.024% after integration convergence, while the refined mesh (SEL=0.025) error is determined to be approximately 0.022%.

4.3 Edge Cracked Bar where Crack is not Aligned with Orthotropy Axis

In this example calculation, the same geometry as in Figure 4 is used and the same finite element models from Figure 5 are used. The difference in this case is that the material properties are rotated on the x-y plane through an angle α. In other words, the crack orientation changes with respect to the material properties. In this example, different orthotropic material properties are used and 32x32x32 integration order is used in order to obtain accurate results.

Orthotropic material properties for a glass-polymer composite were used in this crack analysis. The material properties are given as follows: $E_{11} = 50GPa$ $E_{22} = 15.2GPa$, $E_{33} = 15.2GPa$, $G_{12} = 4.7GPa$, $G_{13} = 4.7GPa$, $G_{23} = 3.28GPa$, $\nu_{12} = 0.254$, $\nu_{13} = 0.254$, $\nu_{23} = 0.428$. These material properties are rotated with $\alpha = 15^0$ increments. The results are plotted in Figure 6 and Figure 7. The stress intensity factors are normalized by $K_0 = \sigma_0\sqrt{\pi a}$. Figure 6 and Figure 7 show the variation of normalized K_I and K_{II} plotted with respect to material rotation angle α. α is defined in Figure 3. It should be mentioned that even when the loading is uniaxial, the crack in this case exhibits a mixed mode behavior. The normalized K_I reaches a

maximum value at $\alpha = 45^0$. Both fine and relatively coarse mesh results are given in Figure 6 and Figure 7. Since there are no reference results for this problem in the literature, the results cannot be compared to a reference value.

It can be seen in Figure 6, normalized stress intensity factor K_I remains unchanged if the material is rotated 90 degrees. The same conclusion was also made in Reference [7].

4.4 A 3-D Orthotropic Plate with a Slanted Crack:

Figure 8 depicts a slanted crack of length *2a* placed in a finite three dimensional plate under constant applied tension σ_0. Figure 9(a) shows the complete finite element mesh used in the numerical calculation. Figure 9(b) shows the detail of the mesh around the two crack tips. The applied load corresponds to σ_{22}=-1000 along the top and bottom edges. Plane strain conditions were enforced on the 3-D models by constraining out-of-plane displacements on the front and back faces. In the model, quadratic elements were used. In the mesh, the size of the crack tip elements are SEL=0.35. The crack length is $a = \sqrt{2}$. The material used in this example is the same as the one used in the second example problem, i.e., $E_{11} = 50GPa$ $E_{22} = 15.2GPa$, $E_{33} = 15.2GPa$, $G_{12} = 4.7GPa$, $G_{13} = 4.7GPa$, $G_{23} = 3.28GPa$, $\nu_{12} = 0.254$, $\nu_{13} = 0.254$, $\nu_{23} = 0.428$.

In the literature, the same problem was solved in 2-D both numerically and analytically. [9,8]. The solutions obtained are compared with those available in the literature. The results are normalized by the reference analytical value in [9]. The normalized stress intensity factors are plotted as a function of integration order in Figure 10 and Figure 11. The results presented here were obtained by 50x50x50 integration and

the reference values are given in Table 1. It should be noted that the reference analytical value is obtained for an infinite plate.

4.5 Edge Cracked Bar where Crack is not Aligned with Orthotropy Axis with a Material Rotation in y-z Plane

This computational problem is very similar to the one solved in example in 4.2. In section 4.2 the material properties were rotated in x-y plane. The purpose of now rotation the material properties in the y-z plane is to show the effect this rotation on the K_{III} values. In this example the material rotation has a significant effect on the out-of-plane stresses as well as the K_I, K_{II}, K_{III} values.

The dimensions and mesh used in this fracture analysis are the same as in the previous problem. The boundary conditions required to fix the model in space are shown in Figure 12. The material properties are rotated with 15^0 increments. The material properties used in this example are i.e., $E_{11} = 15.2GPa$ $E_{22} = 15.2GPa$, $E_{33} = 50GPa$, $G_{12} = 3.28GPa$, $G_{13} = 4.7GPa$, $G_{23} = 4.7GPa$, $\nu_{12} = 0.077$, $\nu_{13} = 0.428$, $\nu_{23} = 0.254$. Different meshes were used to ensure the mesh refinement convergence. 32x32x32 integration order was used for the enriched elements and transition elements. It should be noted that in this example plane strain constraints are not used to obtain the free surface effect on the solution of these three-dimensional crack problems. Normalized Stress Intensity Factors K_I and K_{III} at the middle point of the straight crack are plotted as a function of α in Figure 13 and Figure 14.The variation of the normalized stress intensity factors K_I, K_{II}, K_{III} of the crack front is plotted in Figure 14, Figure 15, Figure 16. The stress intensity factors are normalized by $K_0 = \sigma_0\sqrt{\pi a}$.

4.6 Penny Shaped Crack in Orthotropic Material

In this example, the problem a penny shaped crack, placed in an orthotropic material, subjected to uniform tensile loading is examined. In an effort to obtain the solution for a penny shaped crack in an orthotropic material, a quarter circular model was constructed with a crack radius $a = 0.557$ and b=3.0, where b outer radius of the cylindrical. The material properties used in Section 4.3 were used in this example. In order to take advantage of symmetry, the crack is placed on one of the orthotropy planes. It should be noted that if the crack is placed arbitrarily with respect to the orthotropy axes or if the orthotropy axes are rotated in the body, there would not be a symmetry plane. In those cases without a symmetry plane, the whole solid model must be constructed. In the first model, 6400 quadratic elements with 29283 nodes were used. The crack front was uniformly divided into 16 elements. In the second model which is finer, 19200 quadratic elements with 84557 nodes were used to converged the results. The enriched elements and transition elements were integrated using 40x40x40 Gauss integration to get highly accurate results. Figure 18 contains the shape and the dimensions of the geometry and Figure 19 shows the two meshes used in the numerical calculations.

Since there are no results for this problem in the literature, the results can not be compared with a reference value. In Figure 20, the normalized stress intensity factors are plotted as a function the angle from the symmetry plane ($\theta = 0^0$) towards the other symmetry plane ($\theta = 90^0$) as shown in Figure 18. The stress intensity factors are normalized with respect to $K_0 = \sigma_0\sqrt{(\pi a)}$. It is interesting to compare these results with the isotropic solution. As it can be seen in Figure 20, in the isotropic case, the stress

intensity factor K_I is constant, while in the orthotropic material, as expected it varies as a function of θ.

Chapter 5

Conclusion

The detailed general formulation of enriched crack tip elements for three-dimensional crack problems in anisotropic materials was presented. The advantage of using this type of finite element formulation is the ease with which complex three-dimensional problems can be solved without having to generate specialized crack tip meshes. The technique developed in this study will provide more accurate fracture results for a wide variety of composite and anisotropic materials. This will be particularly important for advance engineering applications where anisotropic material selection is inevitable for optimization purposes. The example computational problems presented in this thesis shows that assuming anisotropic materials as if they are isotropic may lead to erroneous results in fracture mechanics calculations and remaining life assessment calculations.

A major advantage of the enriched element formulation over other approaches is seen when more complicated crack tip fields are embedded into the same computational algorithm. Future extensions of this work would include three-dimensional interface cracks, cracks with contacting surfaces, cracks terminating on interfaces in anisotropic materials, etc. Highly accurate solutions can be obtained for stress intensity factors in all of these cases if displacement compatibility is ensured using transition elements and integration convergence is verified in the enriched elements.

Tables

Table 1

Stress Intensity Factor for 3-D plate with slanted crack (+, - designates upper and lower crack tips)

Reference	K_I^+	K_{II}^+	K_I^-	K_{II}^-
Sih et.al. [9]	1.0539	1.0539	1.0539	1.0539
Kim et.al [8](MCC)	1.0670	1.0440	1.0670	1.0440
This study	1.0710	1.0591	1.0710	1.0591

Figures

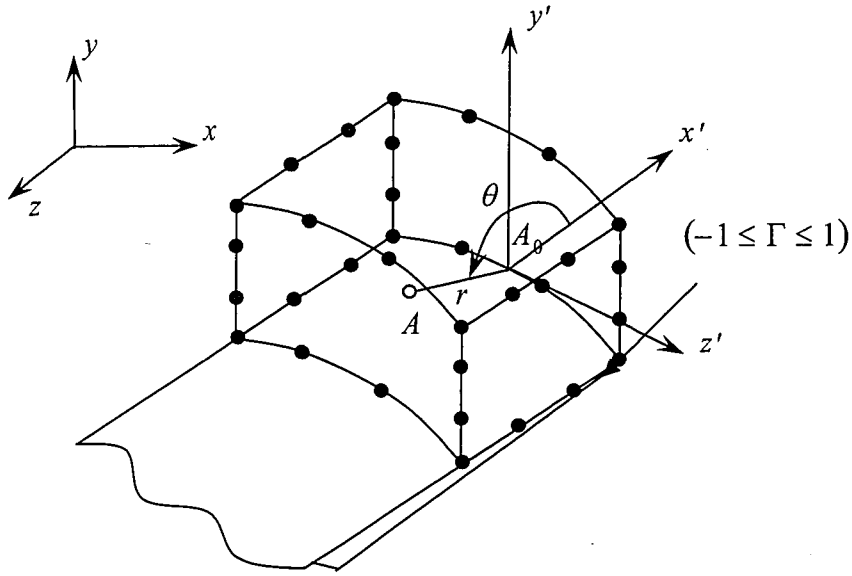

Figure 1: Cubic crack tip element (32-noded hexahedron), showing orientation of local crack tip coordinate system with respect to global coordinates.

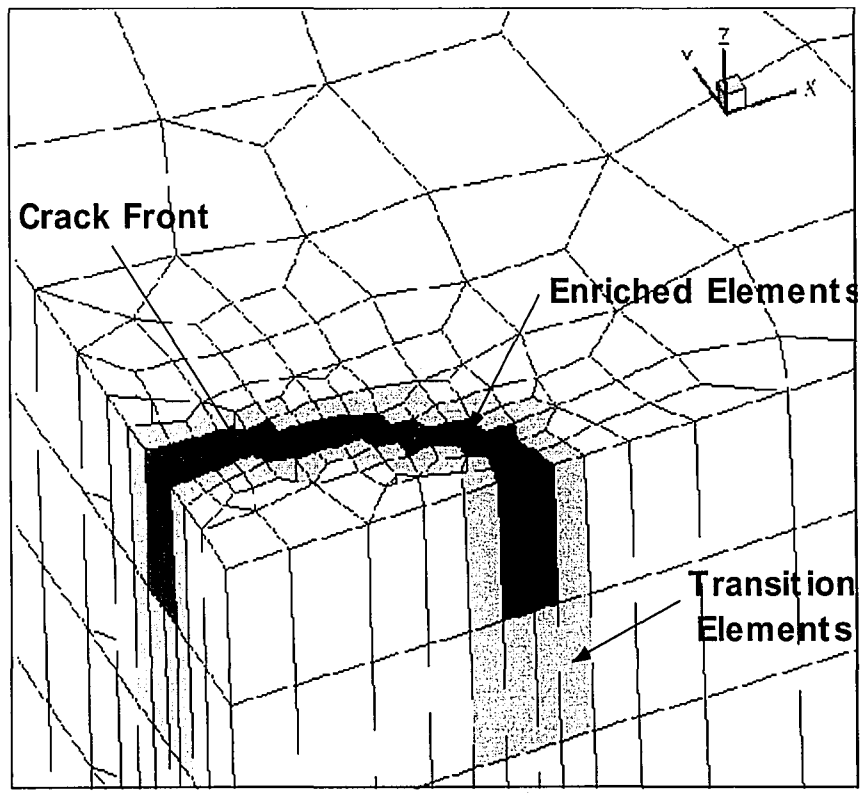

Figure 2: Semi-elliptic surface crack showing enriched elements along crack front and adjacent transition elements. Symmetry plane on the left side of figure.

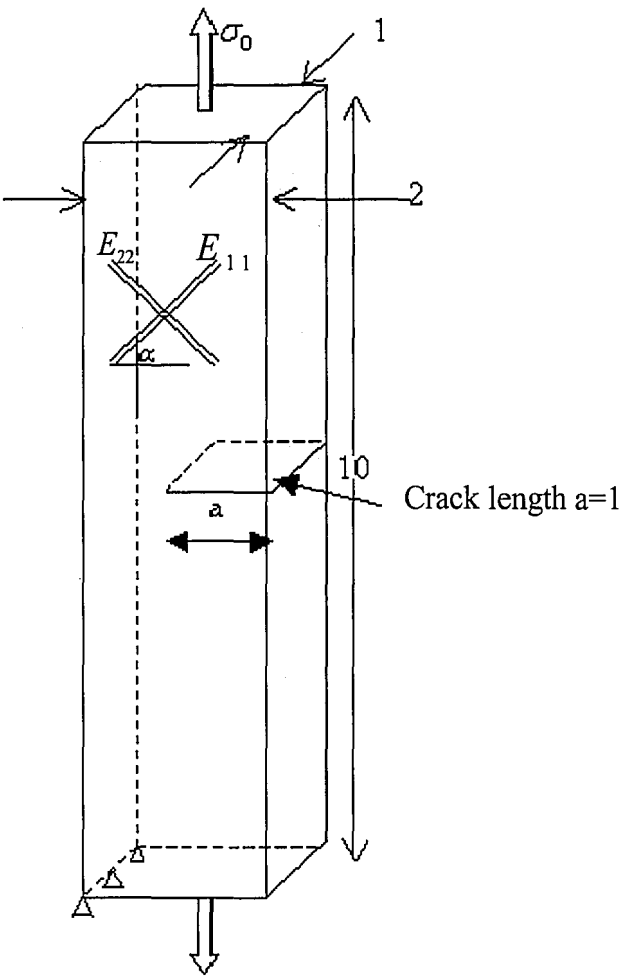

Figure 3. Schematic sketch of edge cracked bar.

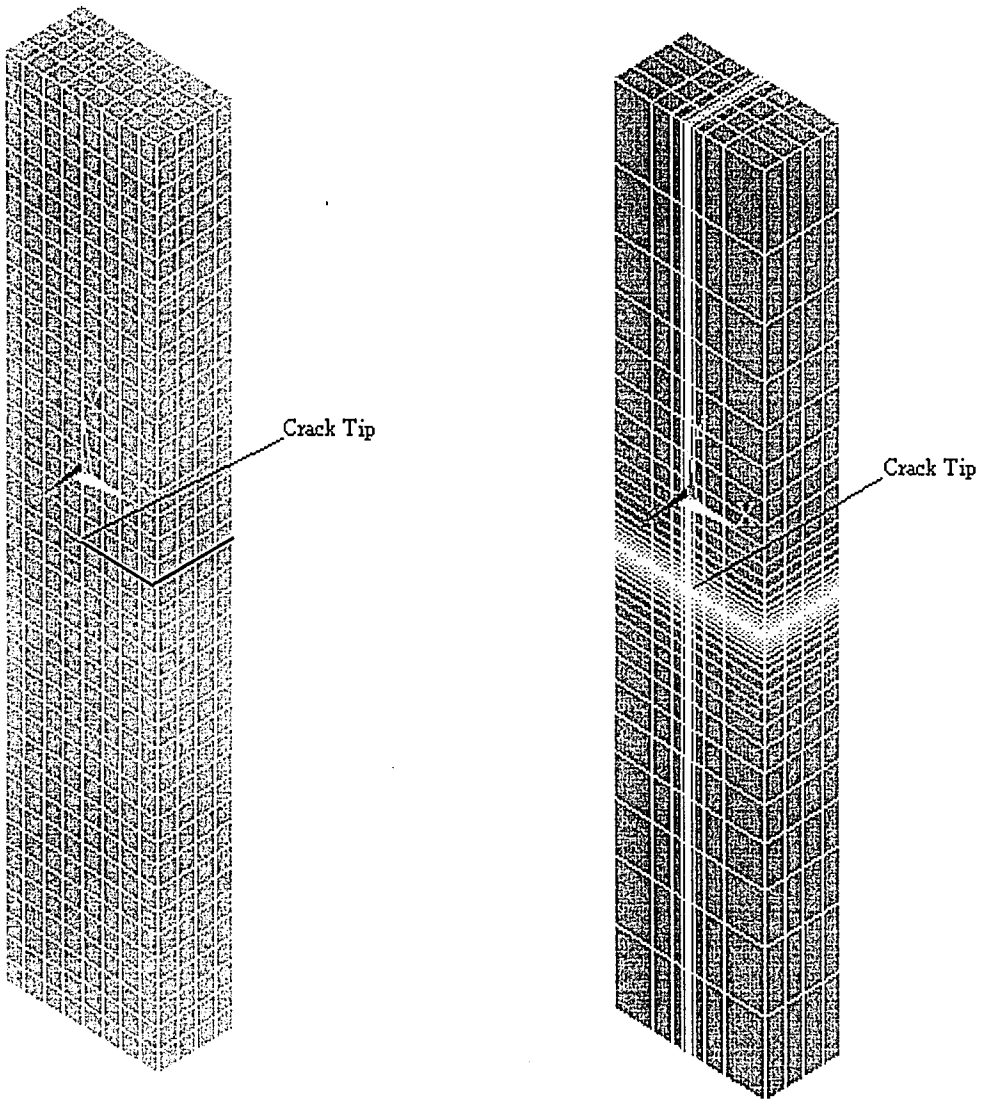

Figure 4. Meshes used in Edge Cracked bar Problem. Crack length a=0.5h where h is the width of the bar. Size of the edge Length (SEL) for crack tip elements in mesh on left is SEL=0.25 and SEL=0.025 for refined mesh on right

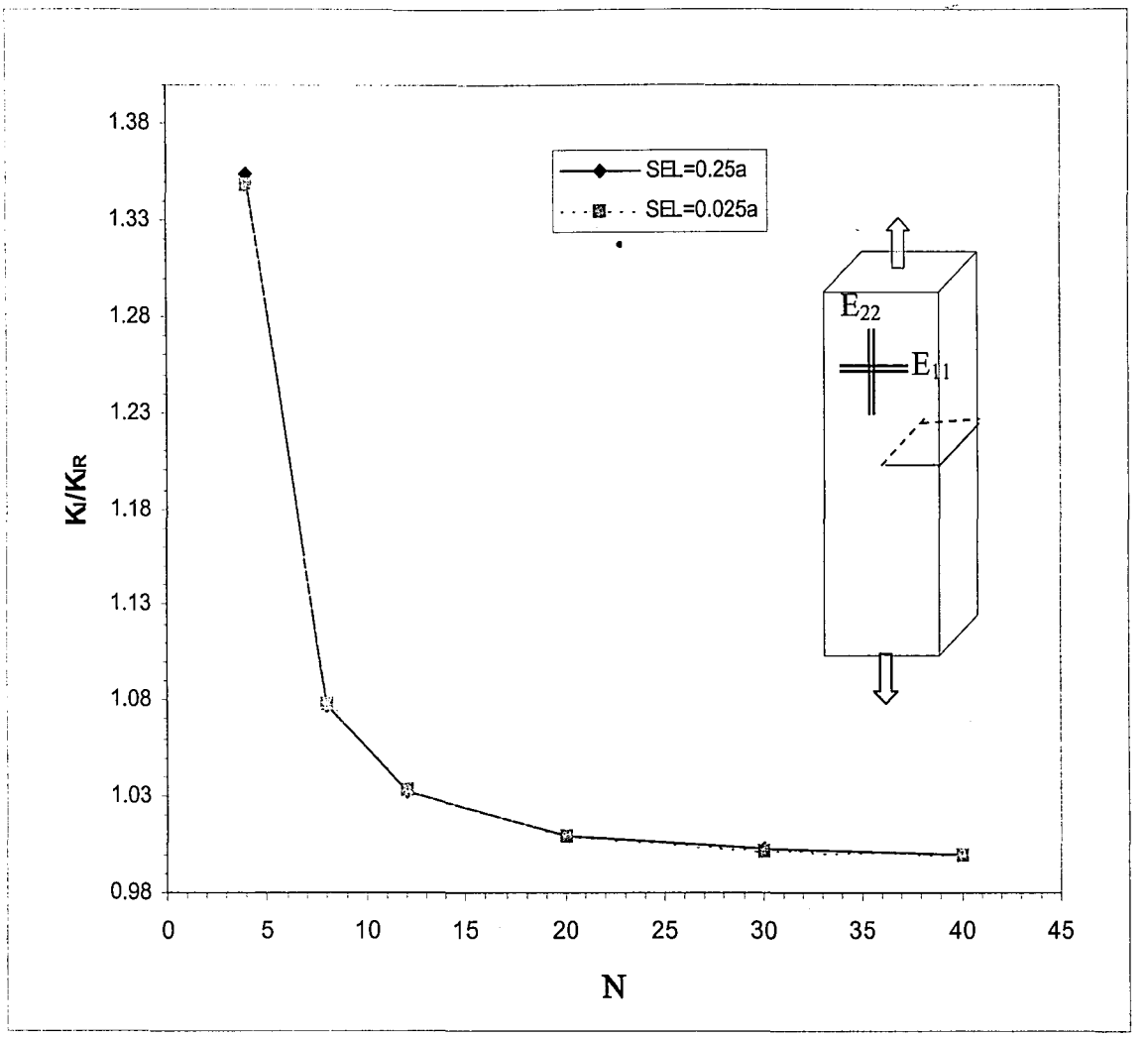

Figure 5. Normalized Stress Intensity factors for plane strain edge cracked bar (a/h=0.5) as a function of Gaussian integration order, including the effect of localized mesh refinement at the crack tip. $K_{IR} = 2.7199\sigma_0\sqrt{\pi a}$ [7]

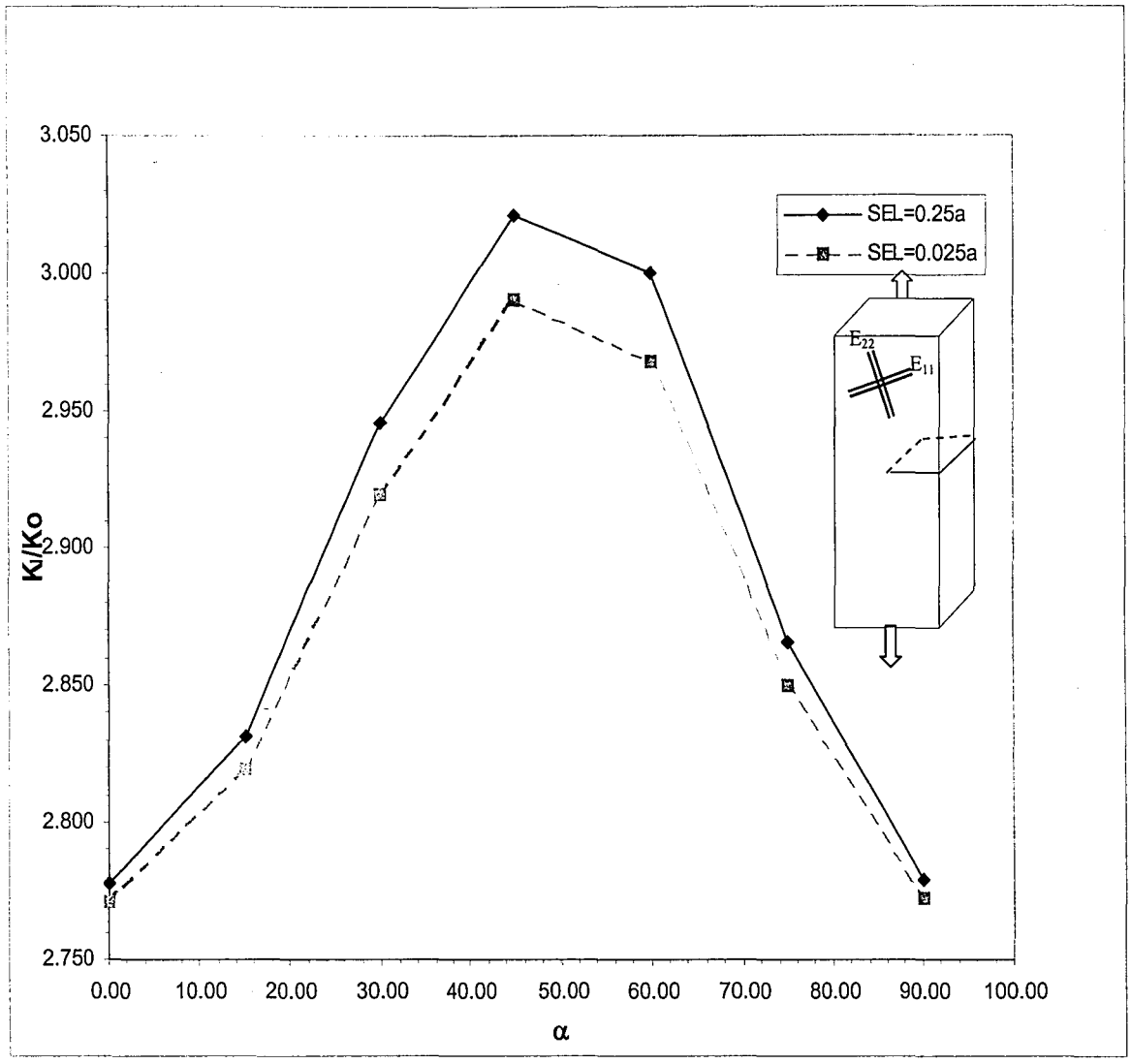

Figure 6. Normalized Stress Intensity factors (K_I) for plane strain edge cracked bar (a/h=0.5) as a function of material orientation α, including the effect of localized mesh refinement at the crack tip. $K_0 = \sigma_0\sqrt{\pi a}$

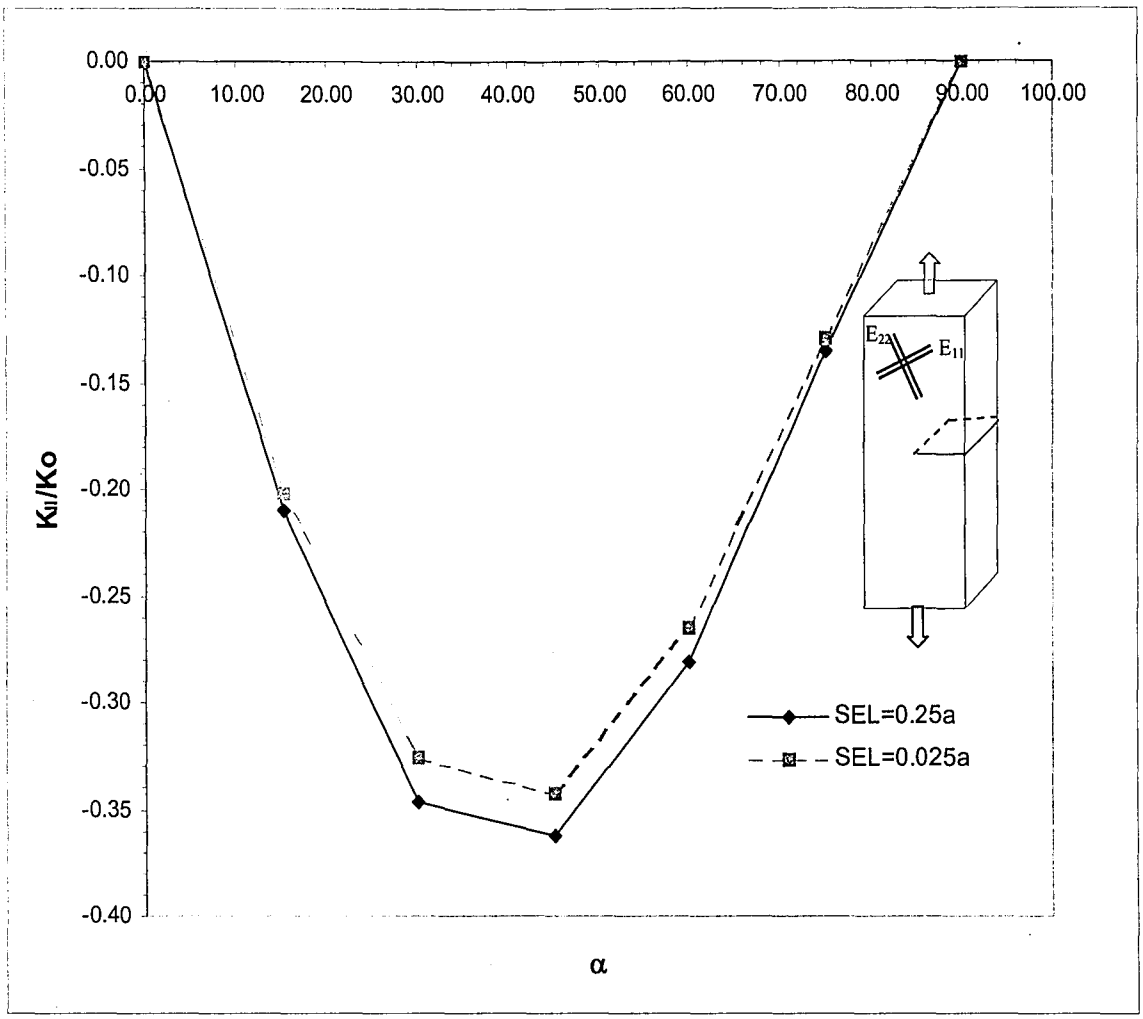

Figure 7. Normalized Stress Intensity factors (K_{II}) for plane strain edge cracked bar (a/h=0.5) as a function of material orientation α, including the effect of localized mesh refinement at the crack tip. $K_0 = \sigma_0\sqrt{\pi a}$

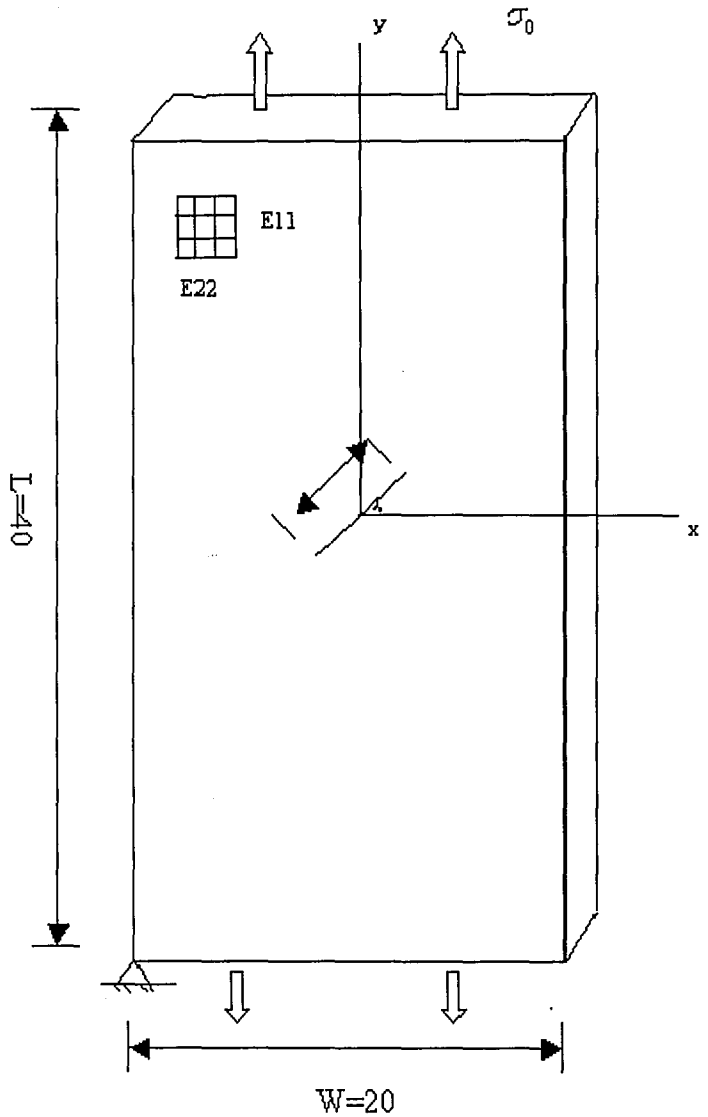

Figure 8. Schematic sketch of geometry of 3-D plate with slanted crack

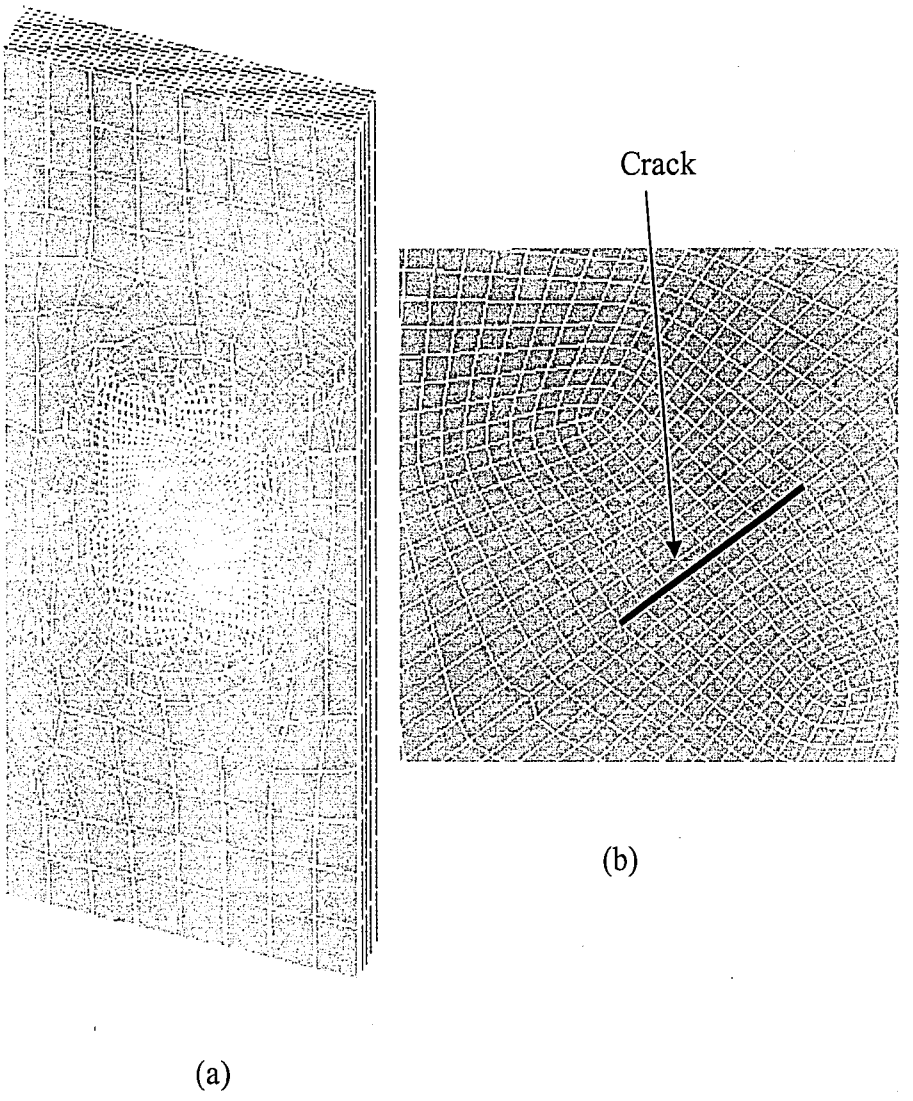

Figure 9. Mesh used in Plate with slanted Cracked Problem. Crack length $a = \sqrt{2}$ Size of the edge Length (SEL) for crack tip elements in mesh on left is SEL=0.25

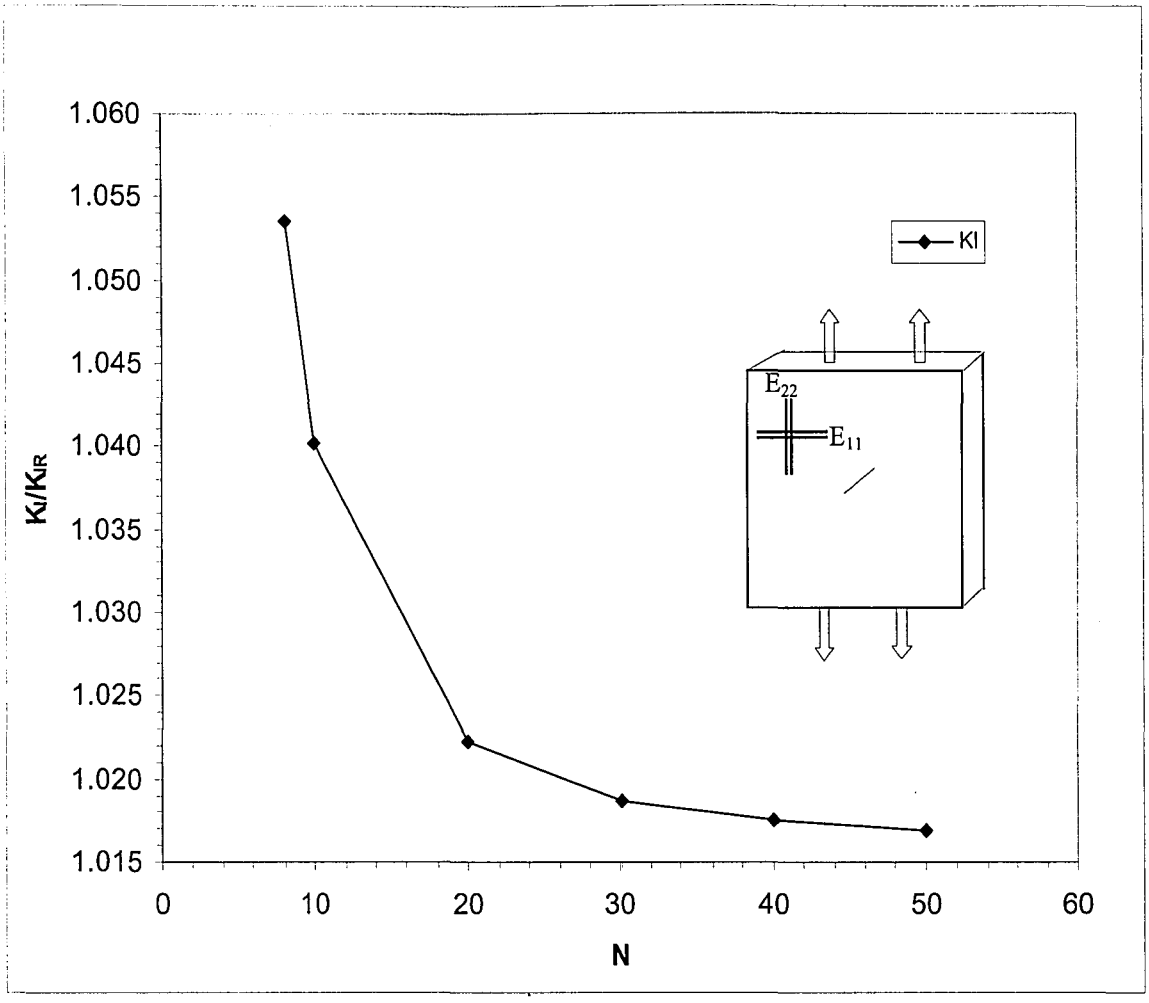

Figure 10. Normalized Stress Intensity factors (K_I) for plane strain plate with slanted crack bar as a function of Gaussian integration order. $K_{IR} = 1.0539\sigma_0$ [9]

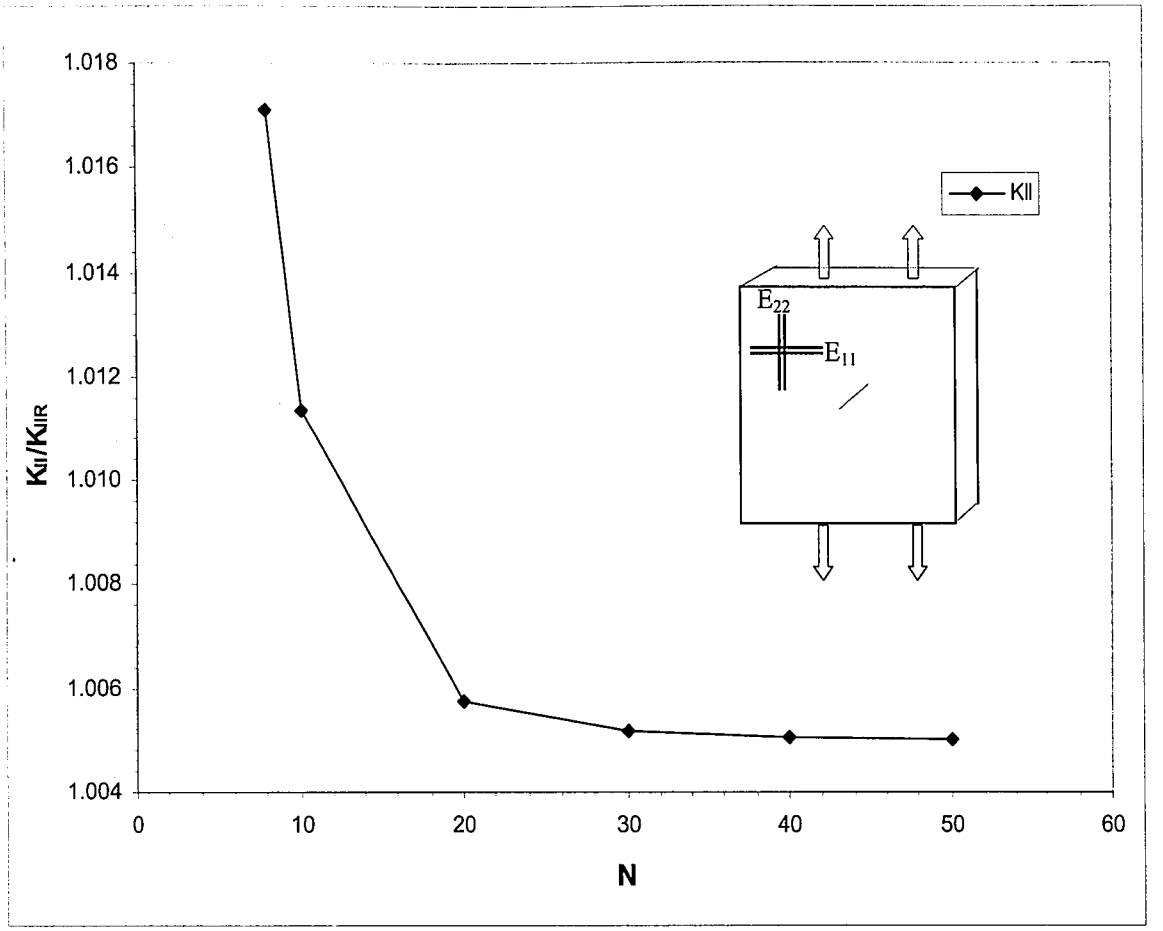

Figure 11. Normalized Stress Intensity factors (K_{II}) for plane strain plate with slanted crack bar as a function of Gaussian integration order. $K_{IIR} = 1.0539\sigma_0$ [9]

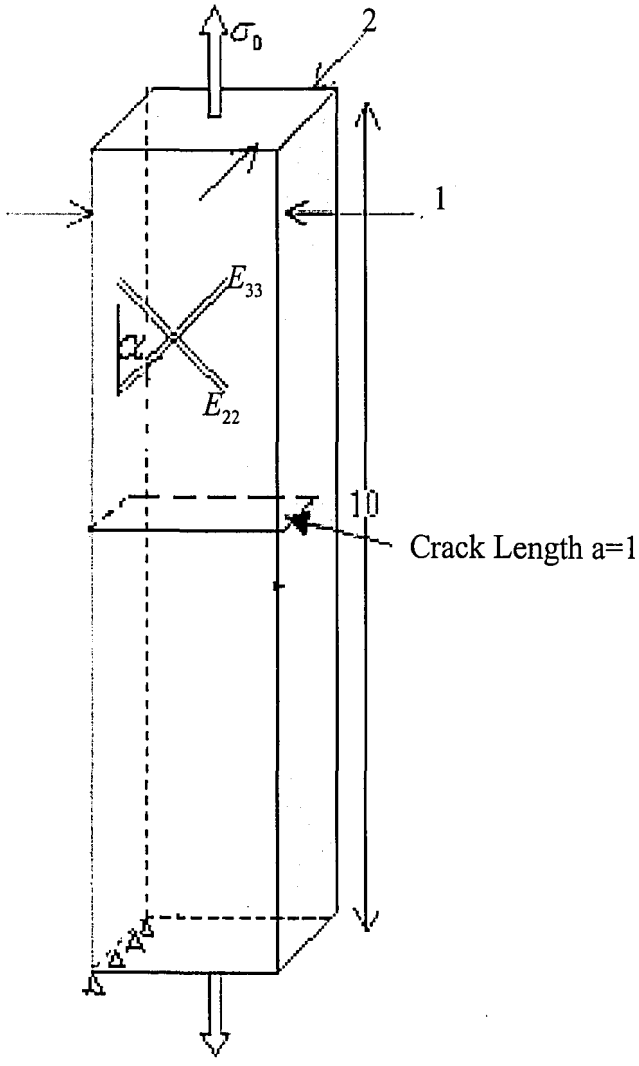

Figure 12. Schematic sketch of geometry of edge cracked bar (different view)

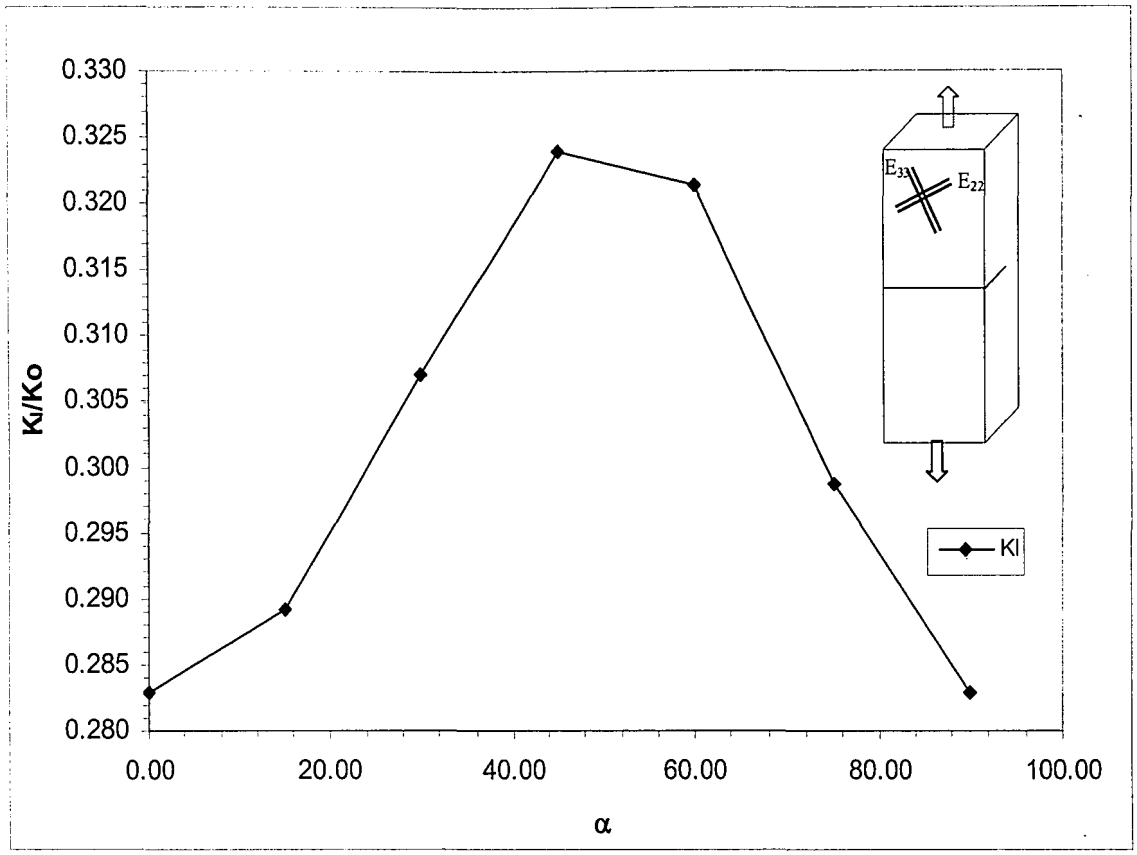

Figure13. Normalized Stress Intensity factor (K_I) of center node of 3-D edge cracked bar (a/h=0.5) as a function of material rotation α . $K_0 = \sigma_0\sqrt{\pi a}$

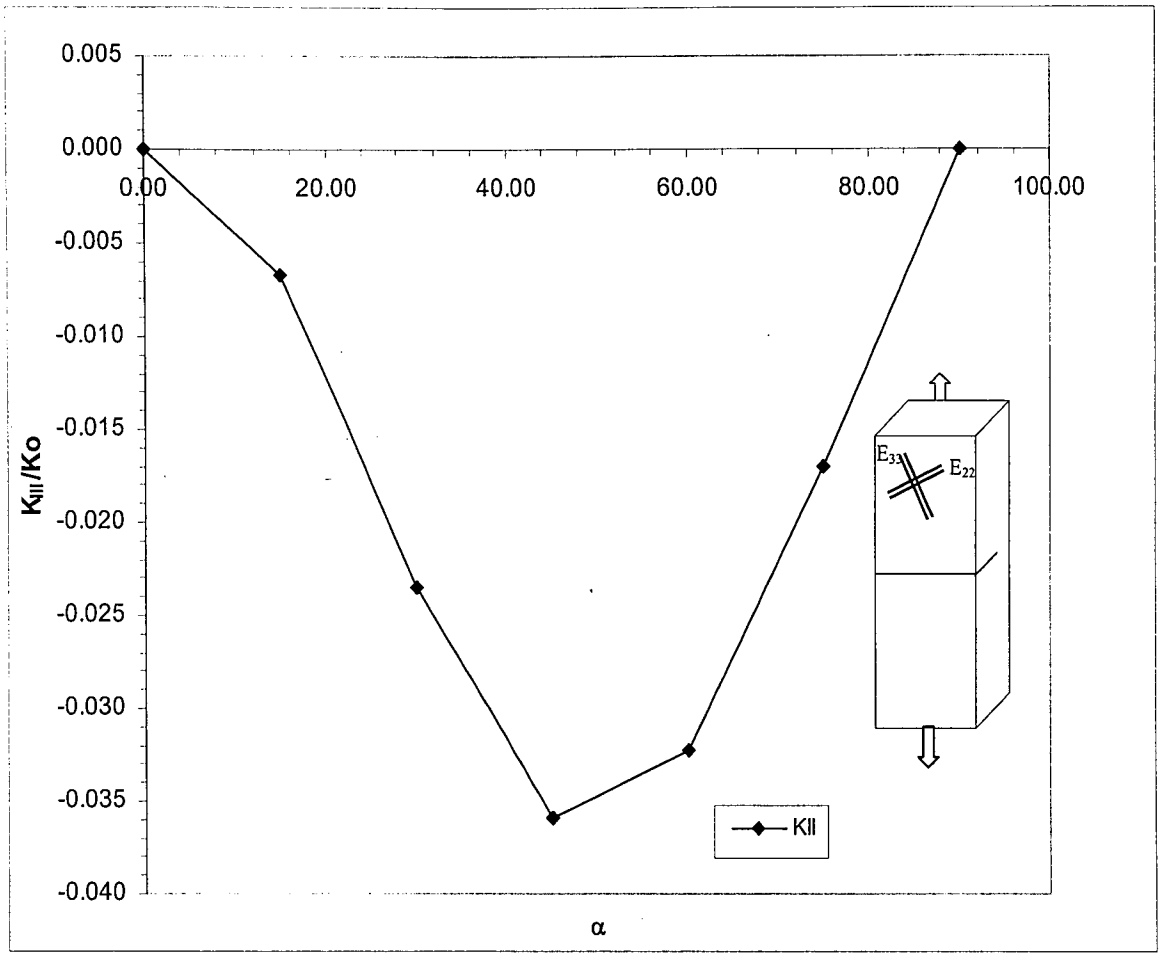

Figure 14. Normalized Stress Intensity factor (K_{III}) of center node of 3-D edge cracked bar (a/h=0.5) as a function of material rotation α . $K_0 = \sigma_0\sqrt{\pi a}$

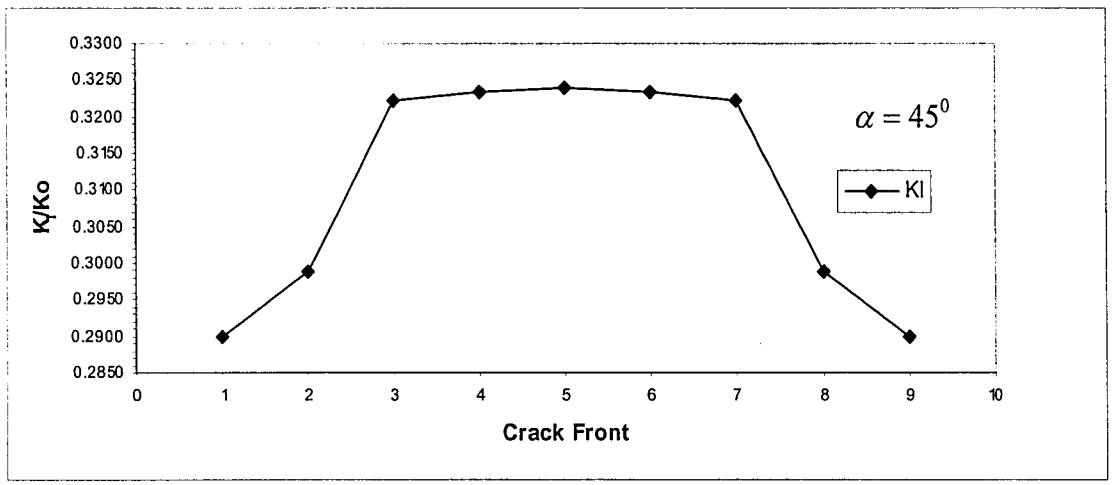

Figure15. Normalized Stress Intensity factor (K_I) of crack front nodes of 3-D edge cracked bar (a/h=0.5), ($\alpha = 45^0$) (no plane strain constraint) $K_0 = \sigma_0\sqrt{\pi a}$

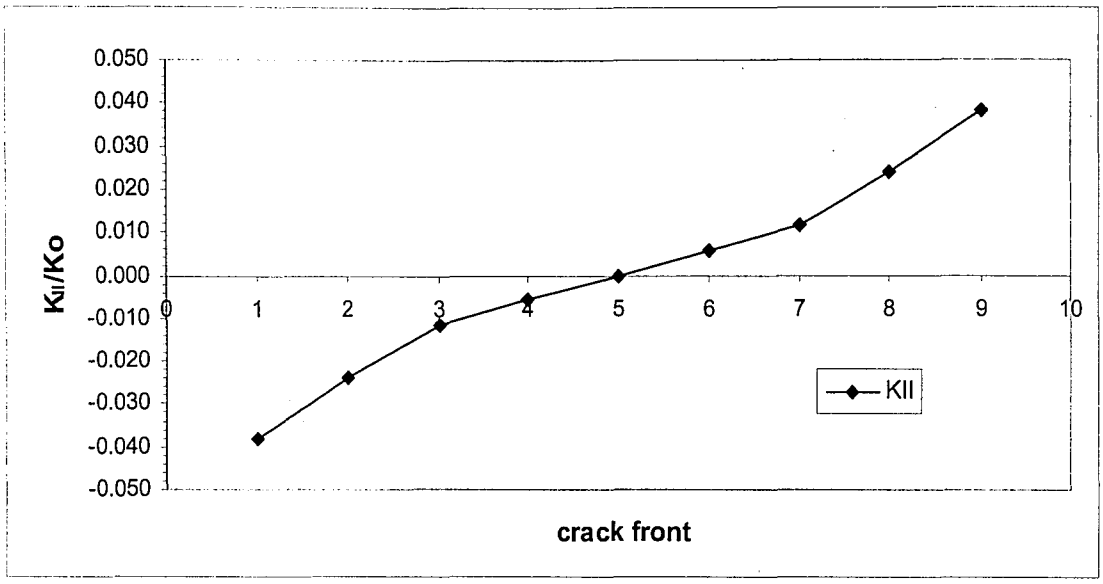

Figure 16. Normalized Stress Intensity factor (K_{II}) of crack front nodes of 3-D edge cracked bar (a/h=0.5),($\alpha = 45^0$) (no plane strain constraint) $K_0 = \sigma_0\sqrt{\pi a}$

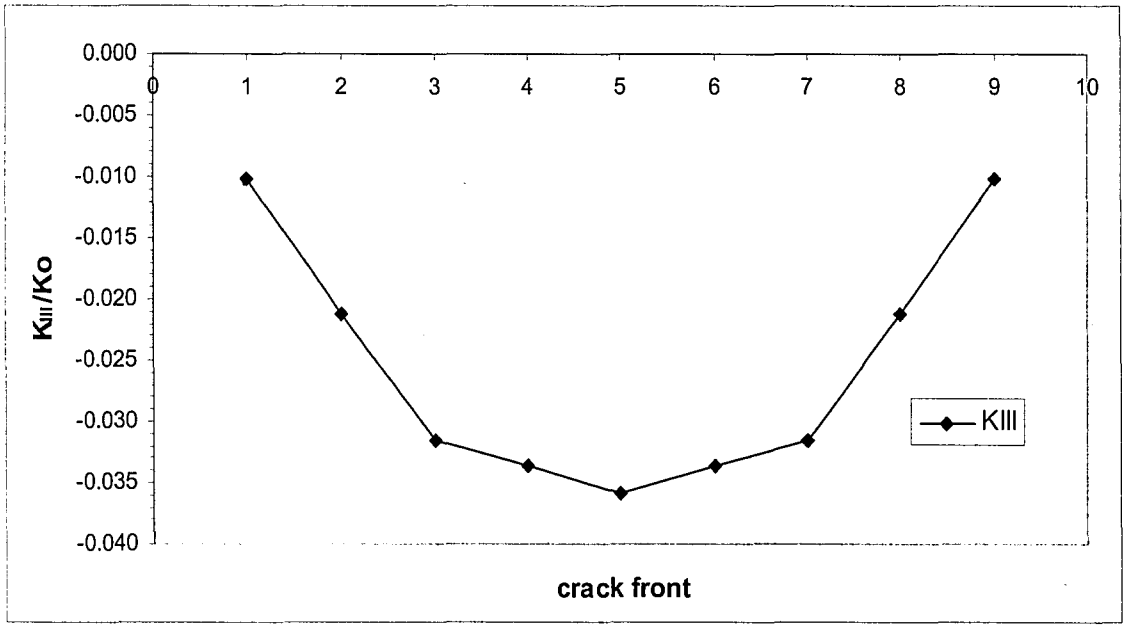

Figure17. Normalized Stress Intensity factor (K_{III}) of crack front nodes of 3-D edge cracked bar (a/h=0.5),($\alpha = 45^0$) (no plane strain constraint) $K_0 = \sigma_0\sqrt{\pi a}$

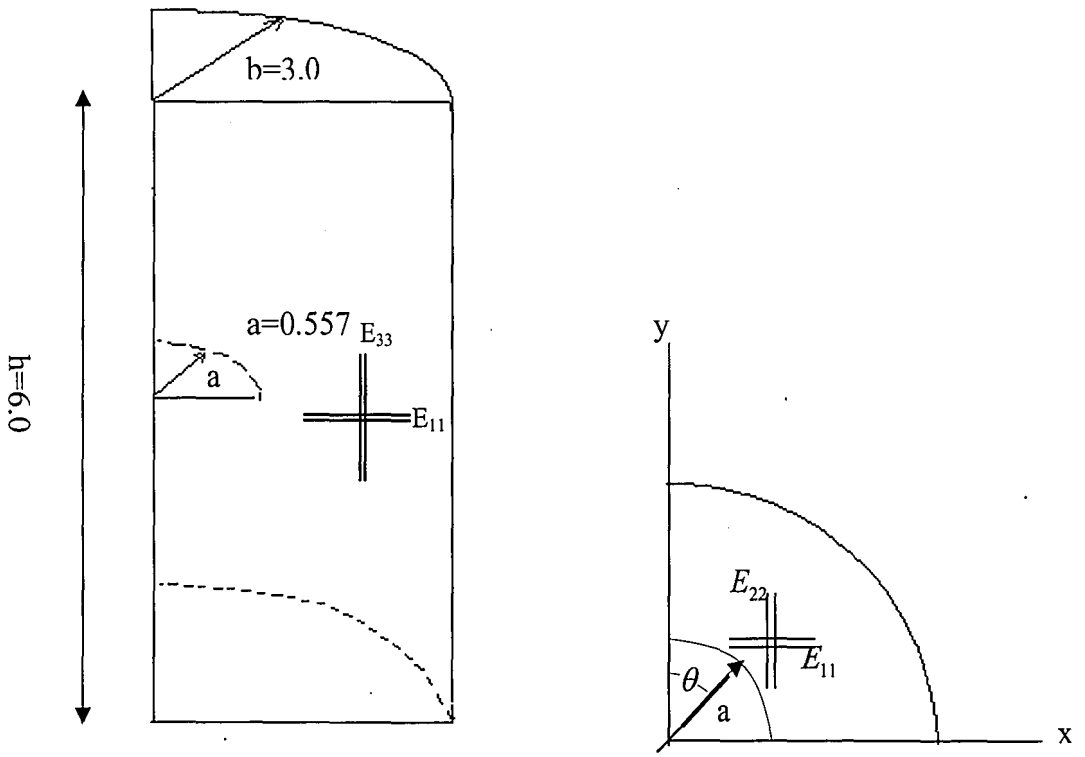

Figure 18. Schematic sketch of orthotropic 3-D circular bar used in penny shaped crack problem. $E_{22} = E_{33}$

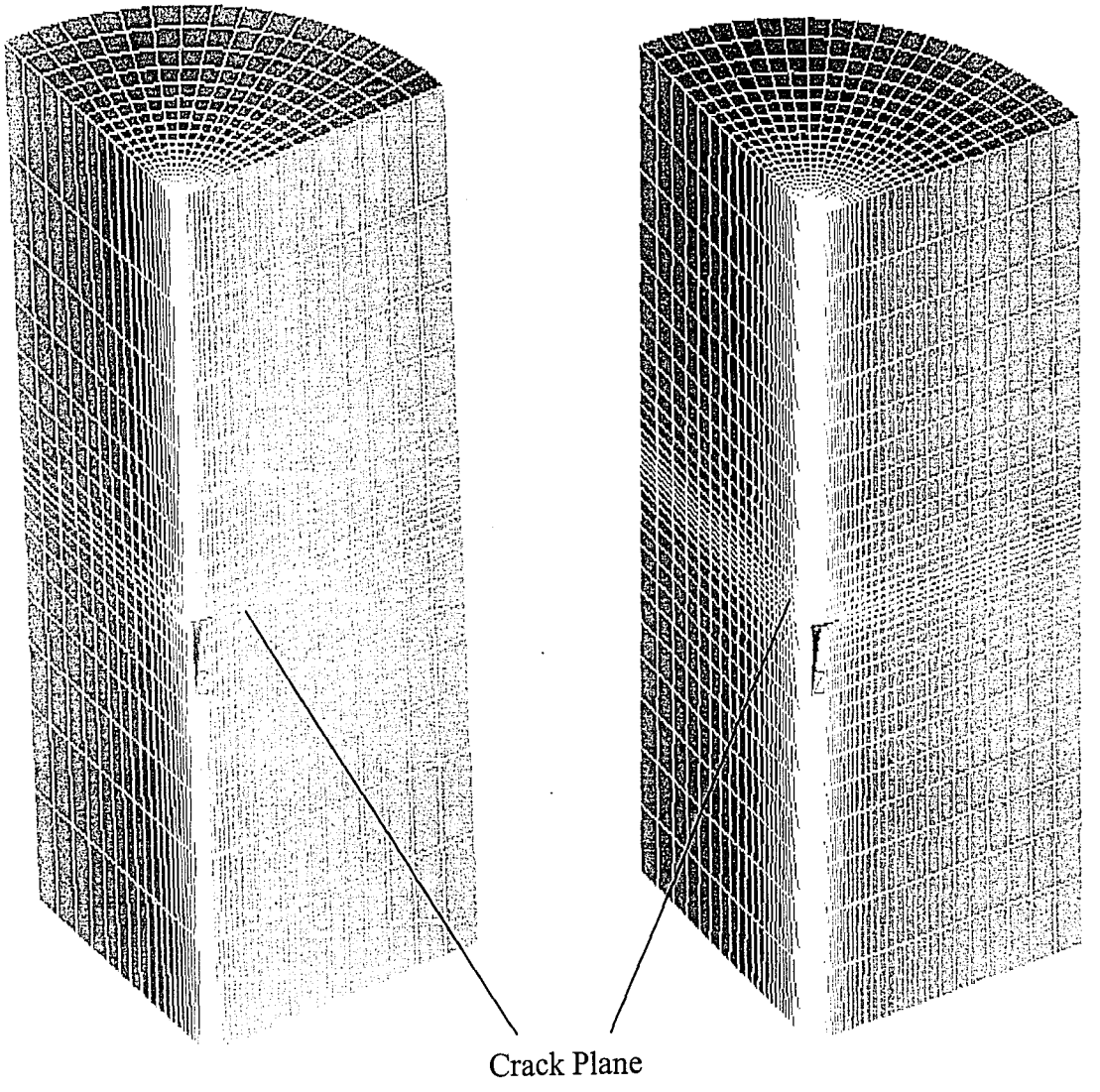

Figure 19. Meshes used in penny shaped crack problem. Crack radius $a = 0.557$ Size of the edge Length (SEL) for crack tip elements in mesh on left is approximately SEL=0.09 SEL for the mesh on the right is approximately SEL=0.05

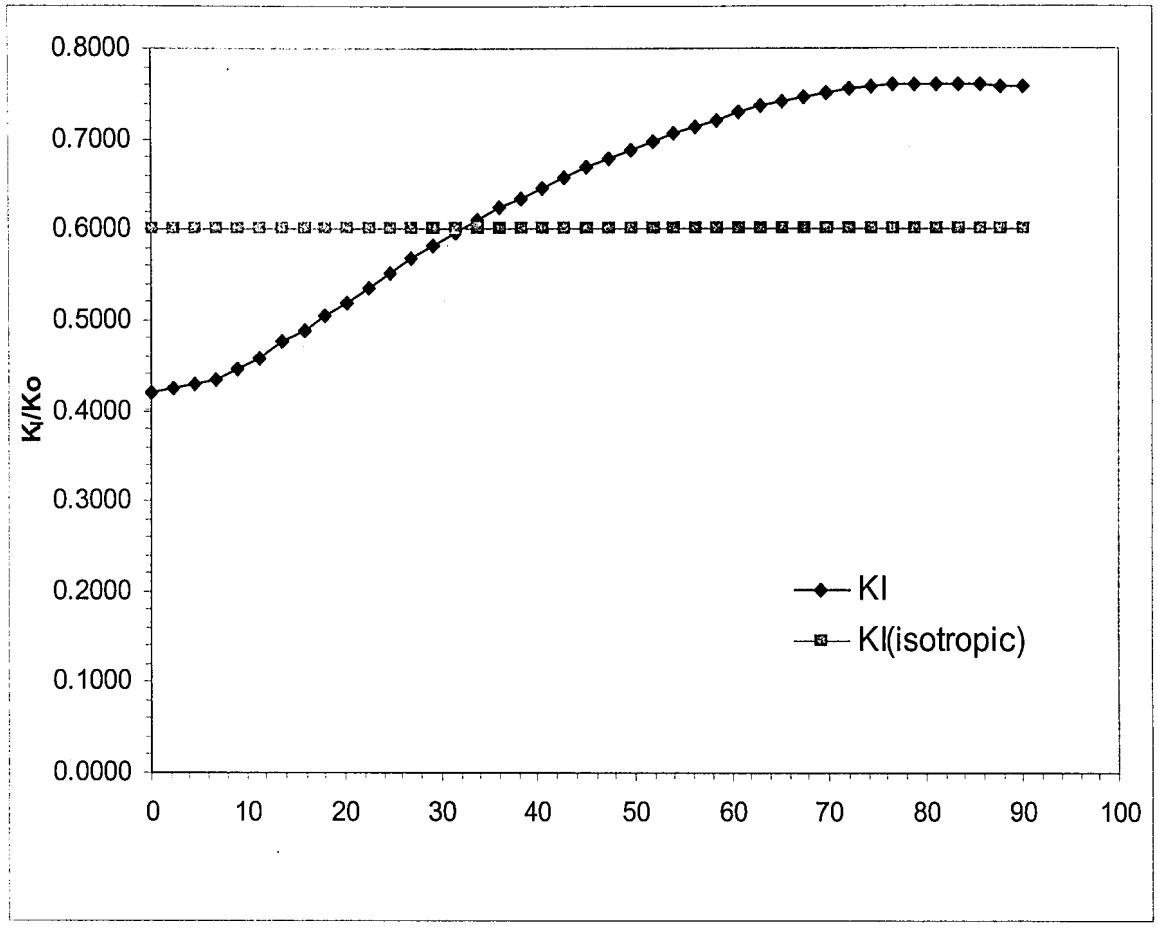

Figure 20. Normalized Stress Intensity factors along crack front for penny shaped crack as a function of the angle from the symmetry plane ($\theta = 0^0$) towards the other symmetry plane ($\theta = 90^0$) and normalized stress intensity factors assuming isotropy. $K_0 = \sigma_0\sqrt{\pi a}$

References:

[1] Ayhan, AO, Nied, HF Stress Intensity Factors for Three-dimensional Surface Cracks Using Enriched Finite Elements. Int. J. Numer. Meth. Engng (2002);54:899-921

[2] Sih, GC and Embley, GT Cracks in anisotropic bodies in a state of generalized plane deformation, Institute of Fracture and Solid Mechanics Technical Report(1970)

[3] Sih, GC, Chen, EP Mechanics of Fracture 6,Cracks in Composite Materials, Martinus Nijhoff Publishers (1981)

[4] Hoenig, A., Near-Tip Behaviour of a crack in a Plane Anisotropic Elastic Body, Engineering Fracture Mechanics Vol.16, No.3, pp393-403 (1982)

[5] Letkhnitskii, S.G., Theory of Elasticity of an Anisotropic Elastic Body, Holdan-Day, San Francisco (1953)

[6] Broberg,KB, Cracks and Fracture, Cambridge University Press, Cambridge (1999)

[7] Kaya,A.c. and Erdogan F., Stress Intensity Factors and COD in an Orthotropic Strip International Journal of Fracture,Vol16,No.2,(1980)

[8] Jeong-Ho Kim, Glaucio H. Paulino, Mixed-mode fracture of orthotropic functionally graded materials using finite elements and modified crack closure method, Engineering Fracture Mechanic 69 (2002) 1557-1586

[9] Sih,G.C.,Paris P.C.,Irwin G.R.,On Cracks in Rectilinearly Anisotropic Bodies, International Journal of Fracture Mechanicsvol1, 189-203 (1965)

[10] Benzley SE. Representation of singularities with isoparametric finite elements. International journal for numerical methods in Engineering 1974;8:537-545

[11] Ayhan, A. O., "Finite Element Analysis of Nonlinear Deformation Mechanisms in Semiconductor Packages," Ph.D. Dissertation, Lehigh University, (1999).

[12] A. C. Kaya and H. F. Nied, "Interface Fracture Analysis Of Bonded Ceramic Layers Using Enriched Finite Elements", Ceramic Coatings, Editor: K. Kokini, ASME MD-Vol. 44, pp. 47-71 (1993).

[13] Zienkiewicz, O. C., The Finite Element Method, 3rd edition, McGraw-Hill, (1977).

Vita

Umit Ozkan was born on Marc 23, 1978 in Yozgat, Turkey to his parents, Guven Ozkan and Ayse Ozkan. He resided in Ankara, Turkey where he attended Gazi Anatolian High School between 1989 and 1996. In fall 1996, he was accepted to Mechanical Engineering in Middle East Technical University, Ankara and graduated with a BS degree in June 2001. He was awarded high honor student for all eight semesters of his undergraduate study. In September, 2001 he started his graduate study in Mechanical Engineering and Mechanics Department, Lehigh University and parallel to this study, he worked as a research assistant in the Institute of Fracture Mechanics with Prof. Herman F. NIED. He will be earning his M.S. in Mechanical Engineering in May of 2003.

END OF TITLE